NDRG2 Deficiency Leads to Attention Deficits and Hyperactive Behaviors

Yan Li, Anqi Yin, Xin Sun, Ming Zhang, Jianfang Zhang, Ping Wang, Rougang Xie, Wen Li, Ze Fan, Yuanyuan Zhu, Han Wang, Hailong Dong, Shengxi Wu, and Lize Xiong

Supplemental Material Index

Supplemental Methods

Home-cage activity.

The animals' home-cage activities were assessed in an open field system as previously described (1). Mice were individually housed and habituated to an experimenter who was blinded to the experimental group 5 days before the test, after which the mice were transferred to the behavioral room with a 12-hour light and dark cycle (lights on from 6:00 to 18:00) and acclimated for 24 hours within their home cages (32.5 × 21 ×16 cm). We then recorded and analyzed their home-cage locomotor activities for 24 hours using a video tracking system (ANY-maze, Stoelting Co., USA).

Gait.

We conducted a gait analysis as previously described (2), with some modifications. Briefly, after a 10-min habituation trial, the forepaws and hindpaws of the mice were painted blue and red, respectively, and the mice were allowed to walk down white paper placed on a 50-cm track. The length and width of each stride were measured by an observer blinded to the mouse genotype.

Muscular strength.

Kondziela's inverted screen test (3) was used to assess mouse muscular strength, with a few modifications. The inverted screen was a 43-cm square of wire mesh consisting of 12-mm squares of 1-mm diameter wire. The screen was surrounded by 4-cm-deep wooden beading (which prevented the occasional mouse from attempting to climb onto the other side). The mice were transferred to the behavioral room 1 hour before testing. The mouse was placed in the center of the

wire mesh screen, and the screen was slowly rotated to an inverted position within 2 sec. The screen was held in a steady position approximately 50 cm above a padded surface. We recorded the time when the mouse fell off, or we removed the mouse when the criterion time of 420 sec was reached. The following scores were used to record the time at which the mouse fell: 1-60 sec = 1, 61-240 sec = 2, 241-420 sec = 3, and more than 420 sec = 4.

Methylphenidate treatment.

Methylphenidate (European Pharmacopoeia, France) was dissolved in 0.9% (w/v) saline to a final concentration of 0.6 g/l. All mice received intraperitoneal injections of methylphenidate (2 mg/kg body weight) or the same volume of saline as a control group. For the activity rescue experiments, the *Ndrg2*$^{-/-}$ mice were treated with methylphenidate 20 min before the open field test.

Brain slice preparations and electrophysiology.

Brain slices were prepared according to the atlas. Mice were anesthetized with 2% isoflurane, and brain slices (300 μm) containing the medial prefrontal cortex, corpus striatum and hippocampus were cut in a vibratome with oxygenated cutting solution containing (in mM): sucrose 252, KCl 2.5, $MgSO_4$ 6, $CaCl_2$ 0.5, $NaHCO_3$ 25, NaH_2PO_4 1.2, glucose 10, VC 1.3, and sodium pyruvate 3. The brain slices were transferred to a recovery chamber in digital circulating water bath (37 °C) with oxygenated ACSF solution (ACSF (in mM): NaCl 124, KCl 2.5, $MgSO_4$ 2, $CaCl_2$ 2, $NaHCO_3$ 25, NaH_2PO_4 1, and glucose 37, pH 7.4). Whole-cell patch-clamp recordings were performed in a recording chamber containing the ACSF solution on the stage of a BX51W1 microscope (Olympus, Japan) equipped with infrared differential interference contrast optics.

EPSCs were recorded from pyramidal neurons with an Axon 700B amplifier (Axon Instruments, United Kingdom), and extracellular stimuli were generated with a bipolar tungsten stimulating electrode. The recording pipettes (4–6 MΩ) were filled with internal solution containing (in mM): Cs-MeS_2O_3 140, $MgSO_4$ 1, NaCl 5, EGTA 0.5, HEPES 10, Mg-ATP 2, Na_3-ATP 0.1, QX-314 2, spermine 0.1, and phosphocreatine 10, pH 7.3. EPSCs of pyramidal neurons were induced by extracellular stimulation at 1 Hz with a holding potential of -60 mV. Tetrodotoxin (1 μM) and picrotoxin (100 μM) were added to the perfusion solution. The access resistance of neurons at 15–30 MΩ was recorded, and the data were not recorded if the access resistance changed by 15% or more. To investigate the receptor sensitivity to exogenous ligand stimulation, glutamate (25 μM) was added to the perfusion solution.

Synaptosomal surface glutamate receptor measurement.

The hippocampi were microdissected from mice brains, pooled together and incubated with ACSF containing 1 mg/ml of sulfosuccinimidyl-6-(biotinamido) hexanoate (Pierce Chemical, Rockford, IL) for 30 min on ice and quenched by three successive washes with ice-cold TBS (50 mM Tris, pH 7.4, 150 mM NaCl). The microdissected tissues were lysed in ice-cold homogenization buffer (10 mM Tris pH 7.6, 320 mM sucrose, 5 mM NaF, 1 mM Na_3VO_4, 1 mM EDTA, 1 mM EGTA, 0.5 mM 4-(2-Aminoethyl)-benzenesulfonyl fluoride hydrochloride, 50 mM antipain HCl, 25 mM leupeptin and 0.5 mg/ml pepstatin). The homogenates were centrifuged at 1,000 x g at 4 °C for 10 min to remove the nuclei and large debris. After centrifugation, an aliquot of 50 ml was removed and designated the “total protein fraction”. The supernatant was further centrifuged at 10,000 x g at 4 °C to obtain a crude synaptosomal fraction. The supernatant was then discarded, and the pellet

was sonicated on ice in lysis buffer (1% Triton X-100, 0.1% SDS, 50 mM Tris pH 7.4, 150 mM NaCl, 2 mM EDTA, 0.5 mM AEBSF, 50 mM antipain HCl, 25 mM leupeptin and 0.5 mg/ml pepstatin). Samples were subsequently centrifuged at 16,000 x g at 4 °C for 20 min. To isolate biotinylated proteins, 150 mg of protein was incubated with 50 ml of NeutrAvidin agarose (Pierce Chemical, Rockford, IL) for 4 hours at 4 °C. The NeutrAvidin beads were subsequently washed 3 times with lysis buffer, and proteins were eluted off the beads using 40 ml of 2 X SDS-PAGE loading buffer and boiling for 5 min. Both "surface" and "total" protein fractions were separated on 10% SDS-PAGE gels and transferred onto nitrocellulose membranes (Thermo Scientific, USA).

Detection of TAT-NDRG2 (141-160) uptake in vitro.

TAT-NDRG2 (141-160)-FITC (20 μM) was added to the WT astrocyte cultures. FITC fluorescence was used to monitor the peptide uptake by astrocytes with a live-cell imaging system (Olympus, Japan).

Supplemental Figures

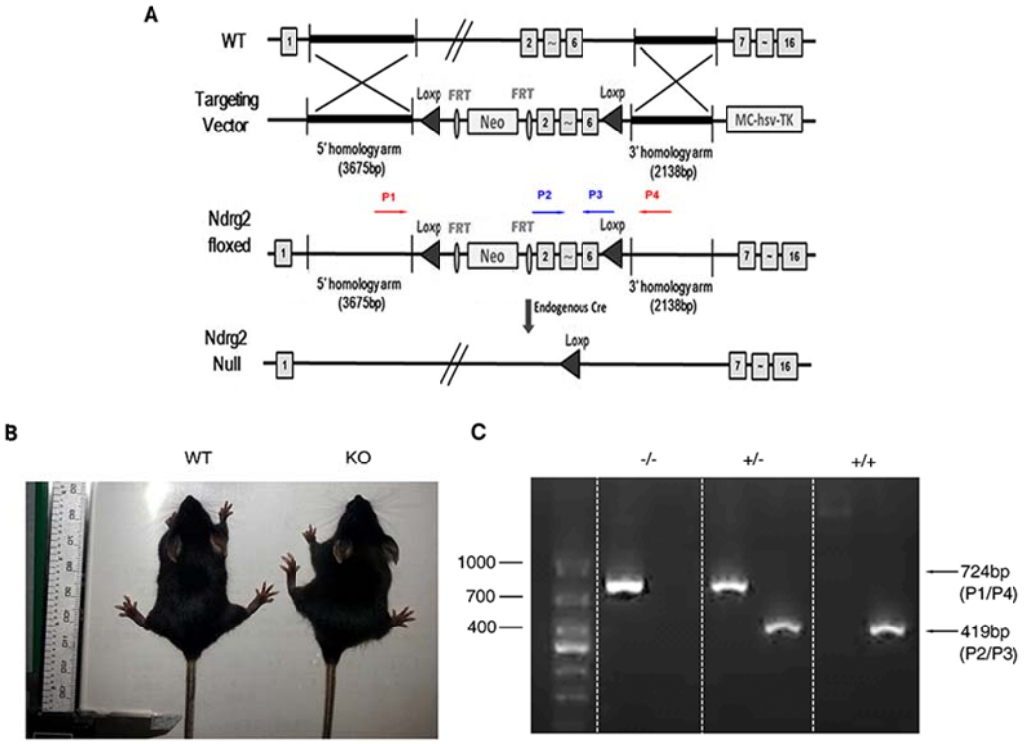

Supplemental Figure 1. Conditional targeting strategy and identification of the *Ndrg2*$^{-/-}$ mice. (**A**) Targeting strategy for the *Ndrg2* conditional knockout (KO) mouse. (**B**) The appearance of an *Ndrg2*$^{-/-}$ mouse and its wild-type (WT) littermate. (**C**) Electrophoretic profiles representing the genotypes of the homozygous *Ndrg2* deletion, heterozygous *Ndrg2* deletion, and WT pattern. The oligonucleotides used for the identification of the *Ndrg2*$^{-/-}$ mice were P1: 5'-AAAAGCTCTCCGTGTGTCTTGGCGT-3'; P2: 5'-GACTCACTCTGTGGAGACACCTT-3'; P3: 5'-CCGCACGAAGTTCTGTATGA-3'; and P4: 5'-GTCATTTGGGAGAATGGAGGAGGCA-3'.

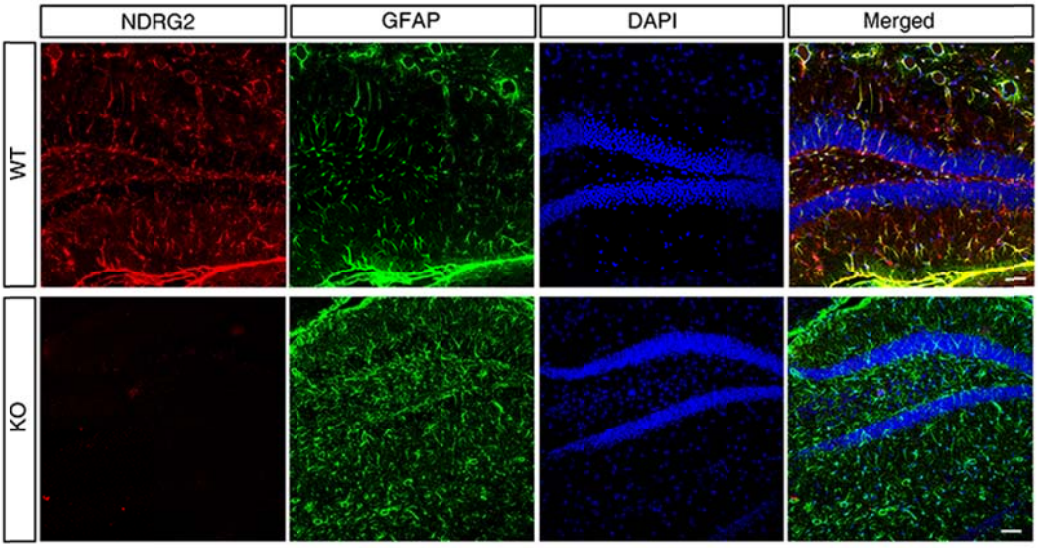

Supplemental Figure 2. NDRG2 is abolished in the KO mice. Representative fluorescence images of NDRG2 (red), GFAP (green), and DAPI (blue) staining in the hippocampi of WT and KO mice. Merged images are shown. Scale bar = 50 μm.

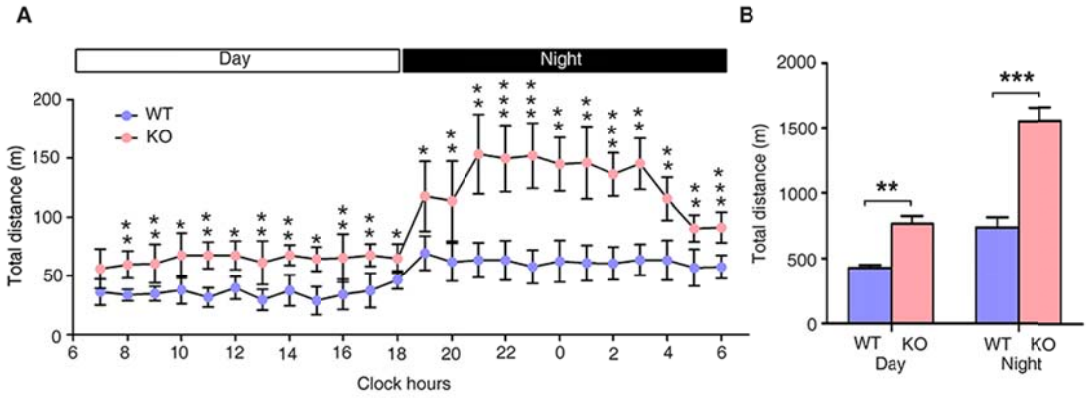

Supplemental Figure 3. Increased home-cage activity in the *Ndrg2*$^{-/-}$ mice. (**A**) The locomotor activity of the two-month-old WT and *Ndrg2*$^{-/-}$ mice in their home cages over 24 hours is presented as the distance traveled per hour. (**B**) The total distance traveled by the WT and *Ndrg2*$^{-/-}$ mice during the day and night is shown. n = 10 KO mice, n = 9 WT mice; error bars, mean ± SEM; $^{*}P < 0.05$, $^{**}P < 0.01$, $^{***}P < 0.001$; Student's *t*-test (**A**) and one-way ANOVA with the Tukey-Kramer *post hoc* test (**B**).

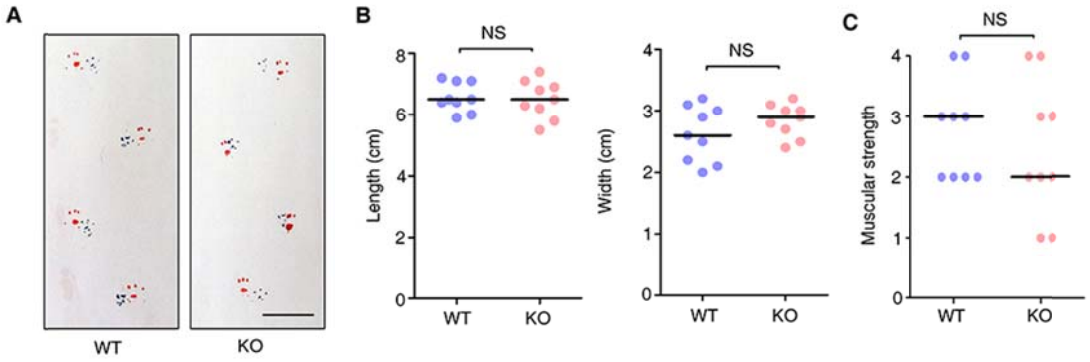

Supplemental Figure 4. Intact stride and muscular strength in the *Ndrg2*$^{-/-}$ mice. (**A**) Representative images of the strides of the WT (left) and *Ndrg2*$^{-/-}$ mice (right) in the gait test (scale bar = 2 cm). Forepaw (red) and hindpaw (blue). (**B**) Quantification of the stride length and width of the hindpaws of the WT and KO mice. (**C**) The muscular strength of the WT and KO mice was measured using Kondziela's inverted screen test. n = 9 KO mice, n = 9 WT mice; horizontal bars, medians; Wilcoxon rank sum test.

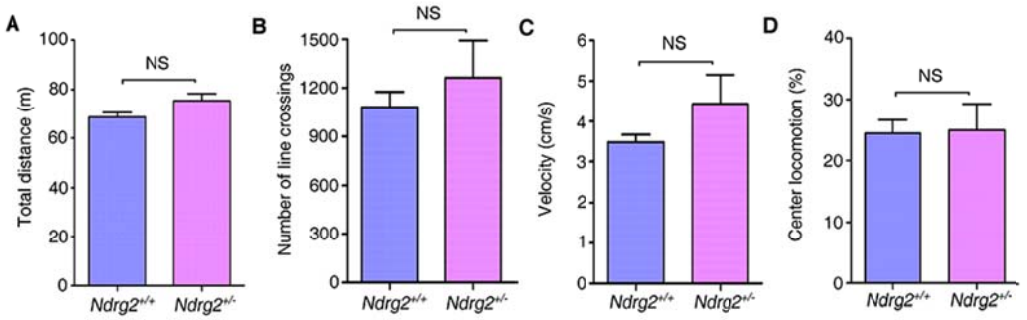

Supplemental Figure 5. Locomotor activity in the *Ndrg2*$^{+/-}$ mice. (**A**-**D**) The locomotor activity of the two-month-old WT (*Ndrg2*$^{+/+}$) and heterozygous (*Ndrg2*$^{+/-}$) mice in an open field is presented as the total distance traveled (**A**), number of lines crossed (**B**), velocity (**C**), and center locomotion (**D**). NS, not significant. n = 8 *Ndrg2*$^{+/+}$ mice, n = 8 *Ndrg2*$^{+/-}$ mice; error bars, mean ± SEM; Student's *t*-test.

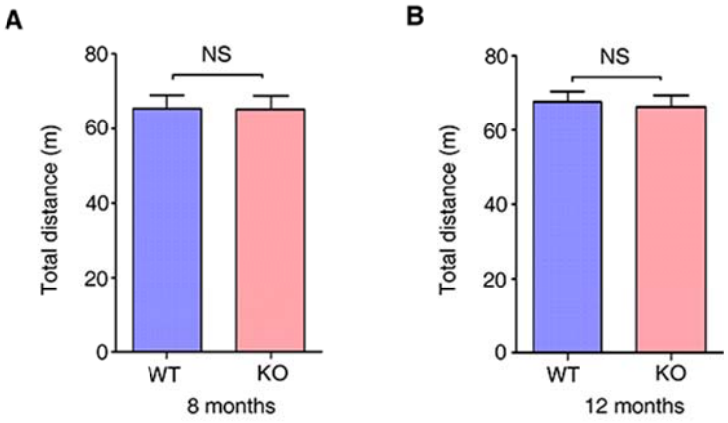

Supplemental Figure 6. Hyperactivity in the *Ndrg2*$^{-/-}$ mice spontaneously subsides at the ages of 8 and 12 months. The locomotor activity of the 8-month-old (**A**) and 12-month-old (**B**) WT and *Ndrg2*$^{-/-}$ mice in an open field is presented as the total distance traveled. n = 7 KO mice, n = 6 WT mice; error bars, mean ± SEM; Student's *t*-test.

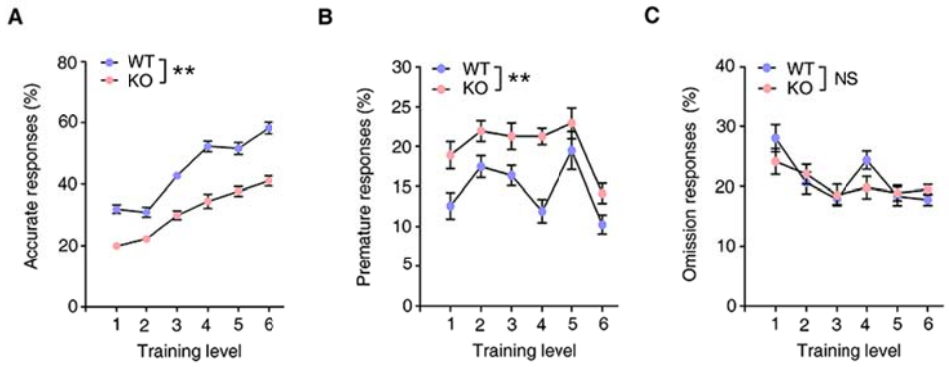

Supplemental Figure 7. *Ndrg2*$^{-/-}$ mice exhibit more incorrect and premature responses during the 5-CSRTT training session. The percentages of accurate (**A**), premature (**B**), and omitted responses (**C**) of the WT and *Ndrg2*$^{-/-}$ mice during the different training sessions are shown. n = 9 per group; $^{**}P < 0.01$; error bars, mean ± SEM; repeated-measures ANOVA.

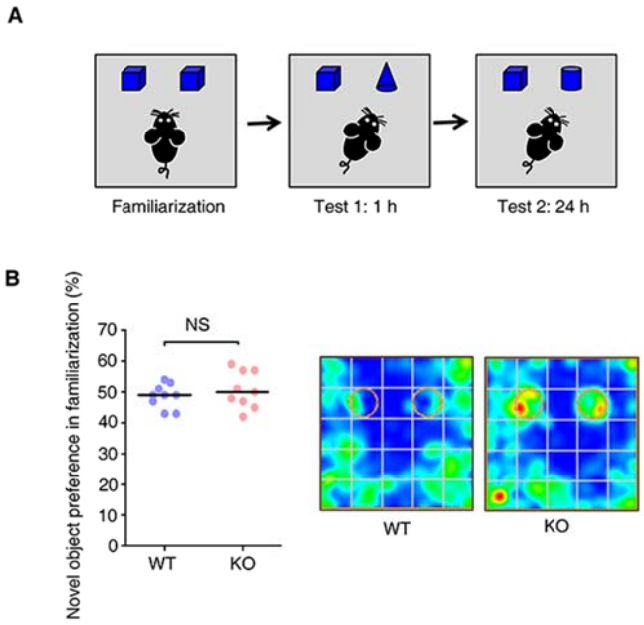

Supplemental Figure 8. Behavioral features in the *Ndrg2*$^{-/-}$ mice in the novel object recognition test. (**A**) Design of the novel object recognition test used to assess short-term and long-term memory. (**B**) In the familiarization phase, the WT and KO mice showed no preference for either of the identical objects. Left: quantification of novel object preference as a percentage. Right: heat maps showing the time spent exploring the identical objects. The circles represent the locations of the objects. n = 9 per group; Wilcoxon rank sum test; horizontal bars, medians.

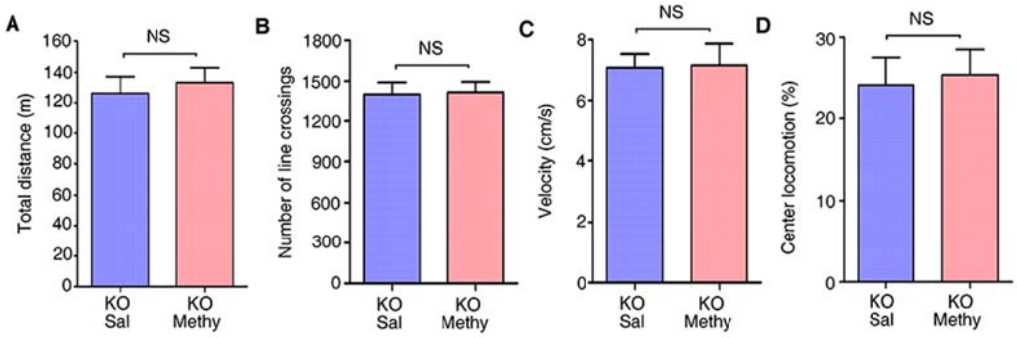

Supplemental Figure 9. Hyperactivity in the *Ndrg2*$^{-/-}$ mice is insensitive to methylphenidate treatment. (**A**-**D**) The locomotor activity in the *Ndrg2*$^{-/-}$ mice treated with saline or methylphenidate in an open field test is shown as the total distance traveled (**A**), number of lines crossed (**B**), velocity (**C**), and center locomotion (**D**). Sal, saline; Methy, methylphenidate. n = 8 KO mice treated with Sal, n = 8 KO mice treated with Methy; error bars, mean ± SEM; Student's *t*-test.

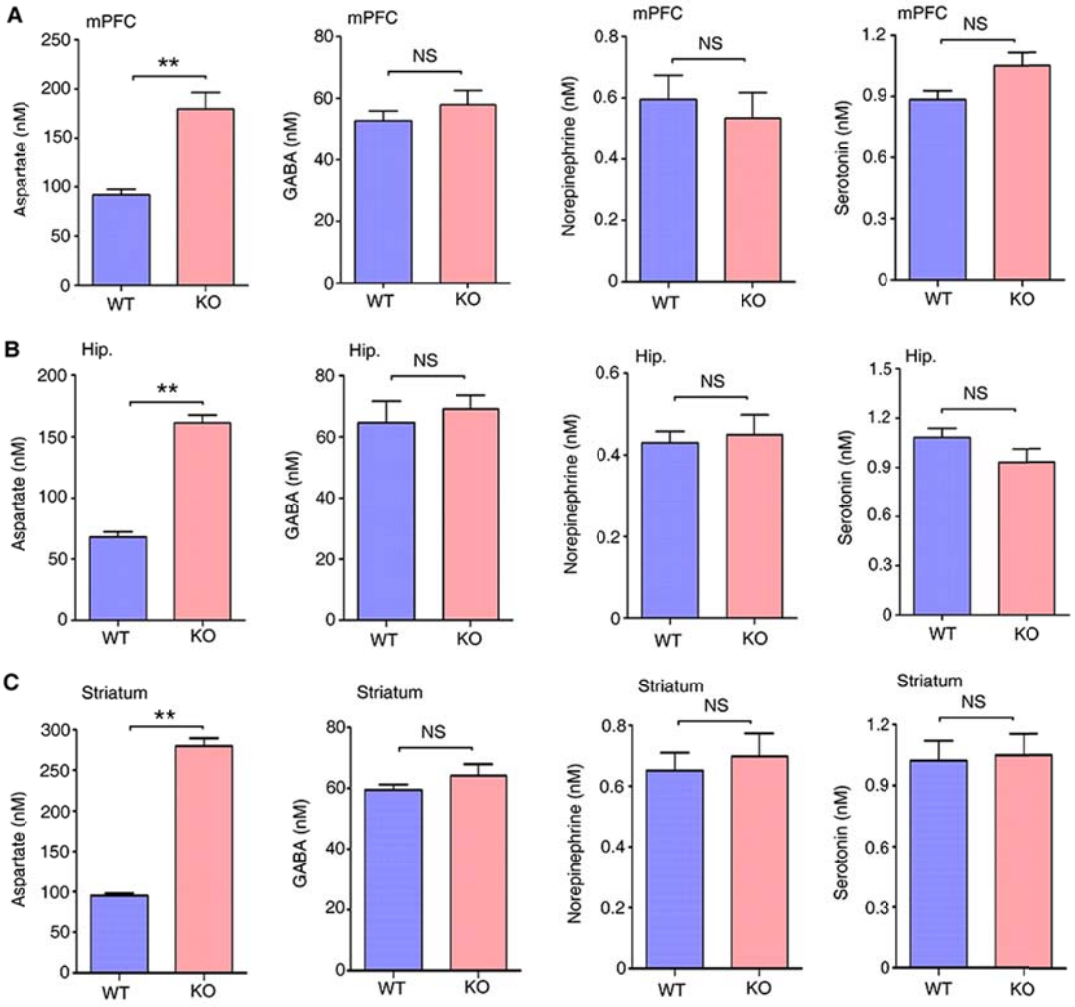

Supplemental Figure 10. Increased aspartate levels in the *Ndrg2*$^{-/-}$ brain at 2 months. Measurements of interstitial aspartate, GABA, norepinephrine, and serotonin concentrations in the mPFC (**A**) hippocampus (**B**), or striatum (**C**) of the WT and *Ndrg2*$^{-/-}$ mice at 2 months. Hip., hippocampus. n = 6 per group; $^{**}P < 0.01$; error bars, mean ± SEM; Student's *t*-test.

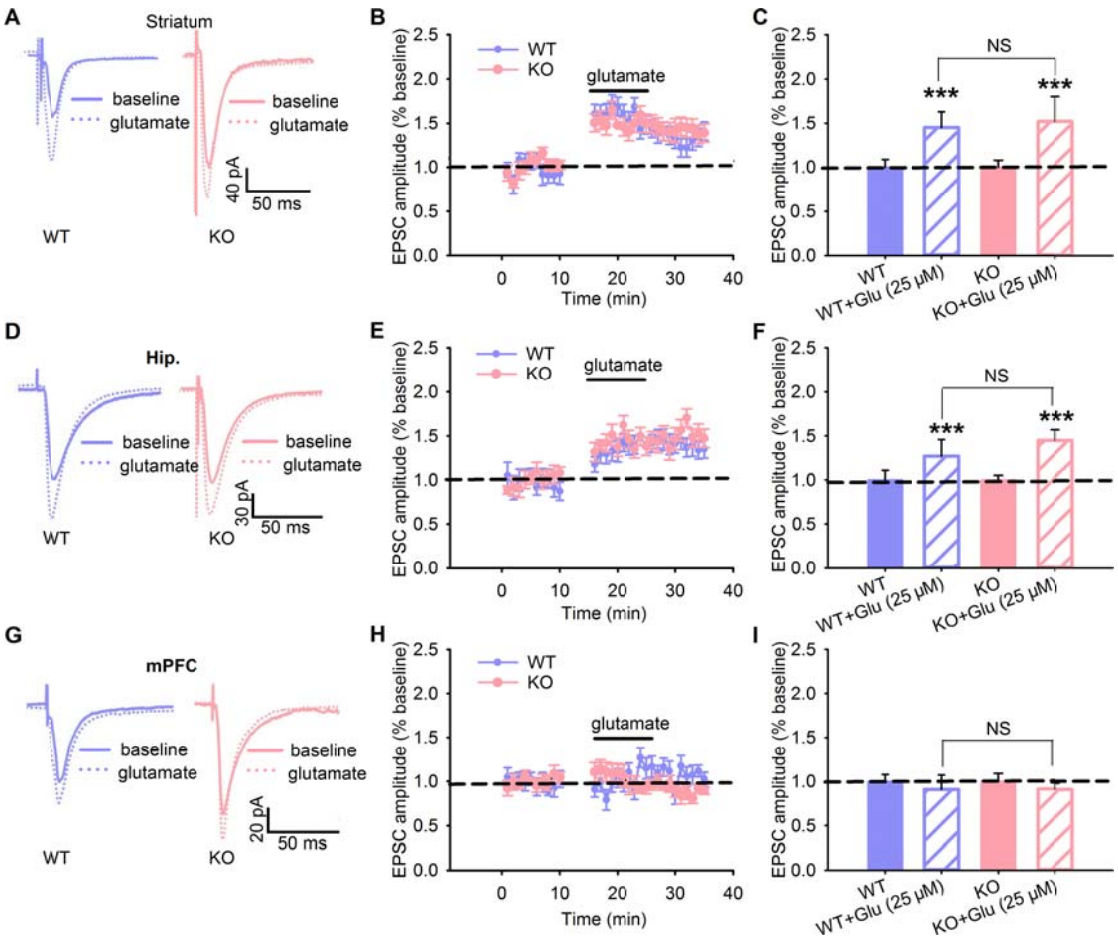

Supplemental Figure 11. Effect of exogenous glutamate on synaptic transmission in the striatum, hippocampi and mPFC of the WT and *Ndrg2*$^{-/-}$ mice. A typical evoked EPSC curve is presented in striatal (**A**), hippocampal (**D**) and mPFC (**G**) pyramidal neurons in WT and *Ndrg2*$^{-/-}$ mice; the effects of exogenous glutamate (25 μM) on EPSC amplitude in three regions are shown in (**B**) (Striatum, WT n=5, KO n=5), (**E**) (Hip., WT n=6, KO n=6) and (**H**) (mPF**C**, WT n=5, KO n=5); and the effects of exogenous glutamate on synaptic transmission are summarized in (**C**), (**F**) and (**I**); Hip., hippocampus; Glu, glutamate; NS, not significant. $^{***}P < 0.001$, compared with the baseline Student's *t*-test; NS, one-way ANOVA with the Tukey-Kramer *post hoc* test.

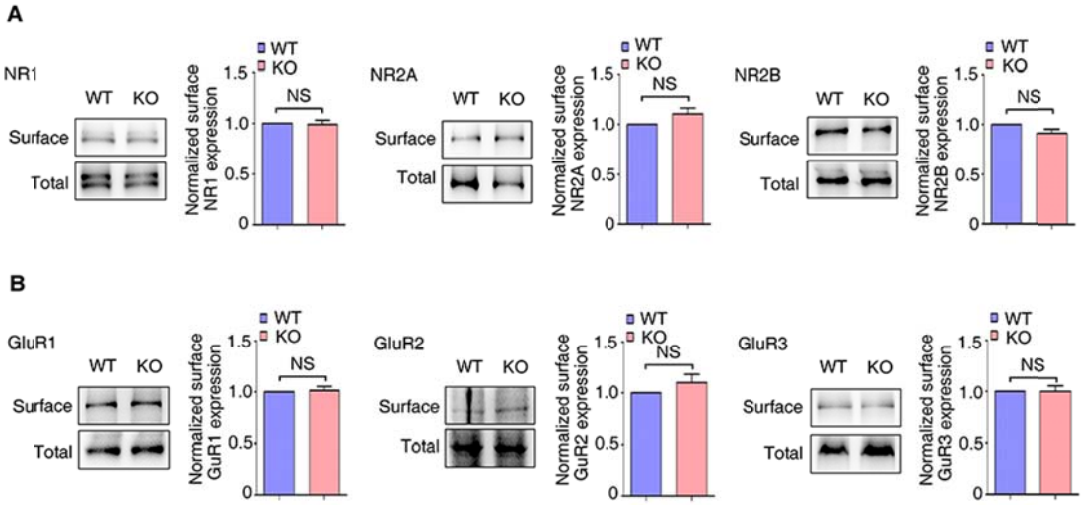

Supplemental Figure 12. Glutamate receptor expression levels in the synaptic membranes in the *Ndrg2*$^{-/-}$ hippocampi at 2 months. Immunoblotting and graphs show the expression levels of NMDARs (NR1, NR2A, and NR2B) (**A**) and AMPARs (GluR1, GluR2, and GluR3) (**B**) at the synaptic surface of hippocampal neurons in the *Ndrg2*$^{-/-}$ mice at 2 months. The synaptic surface protein levels of NMDARs and AMPARs were normalized to the total protein of hippocampal neurons. Representative immunoblots from three independent experiments are shown. Student's *t*-test. Error bars indicate the mean ± SEM.

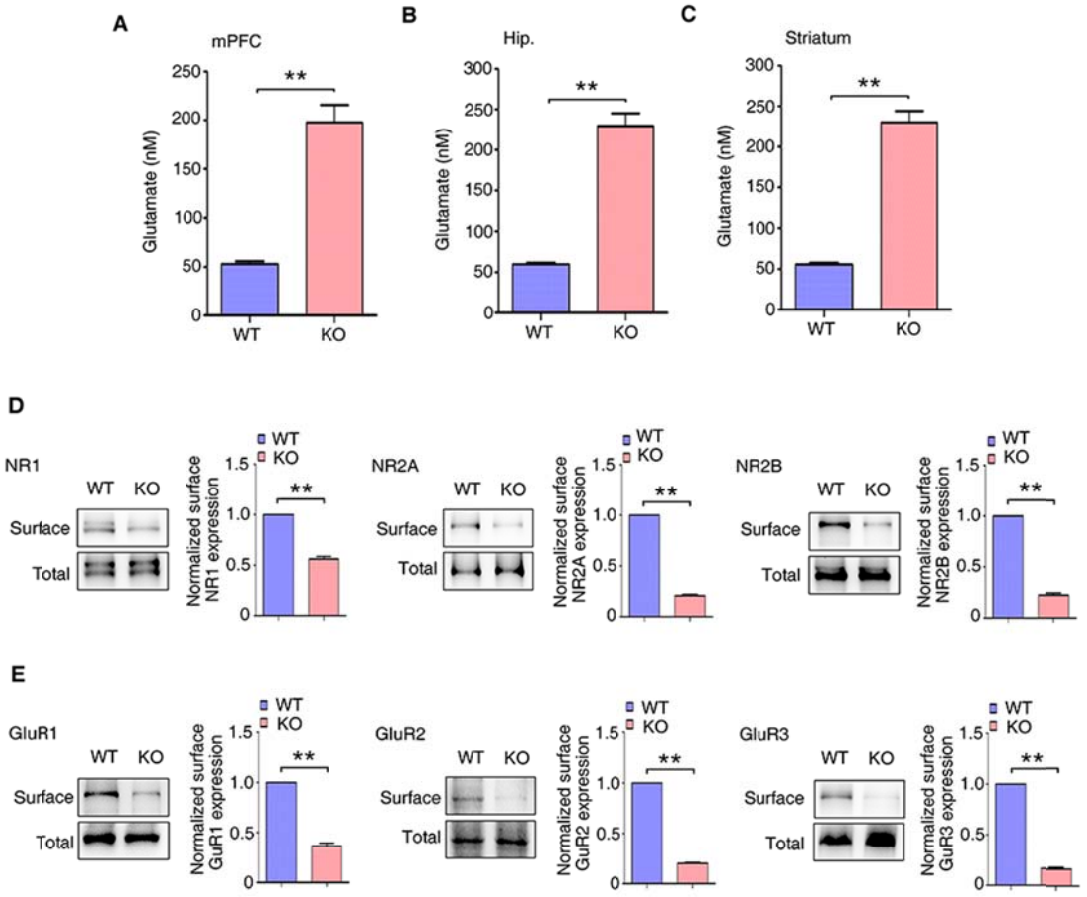

Supplemental Figure 13. Increased glutamate levels and decreased glutamate receptor expression levels in the *Ndrg2*$^{-/-}$ brain at 8 months. Measurements of interstitial glutamate levels in the mPFC (**A**) hippocampus (**B**), or striatum (**C**) in the WT and *Ndrg2*$^{-/-}$ mice at 8 months. Hip., hippocampus. n = 6 per group; $^{**}P < 0.01$; error bars, mean ± SEM; Student's *t*-test. Immunoblotting and graphs show a decrease in NMDARs (NR1, NR2A, and NR2B) (**D**) and AMPARs (GluR1, GluR2, and GluR3) (**E**) at the synaptic surface of hippocampal neurons in *Ndrg2*$^{-/-}$ mice at 8 months. The synaptic surface protein levels of NMDARs and AMPARs were normalized to the total protein of hippocampal neurons. Representative immunoblots from three independent experiments are shown. $^{**}P < 0.01$; Student's *t*-test. Error bars indicate the mean ± SEM.

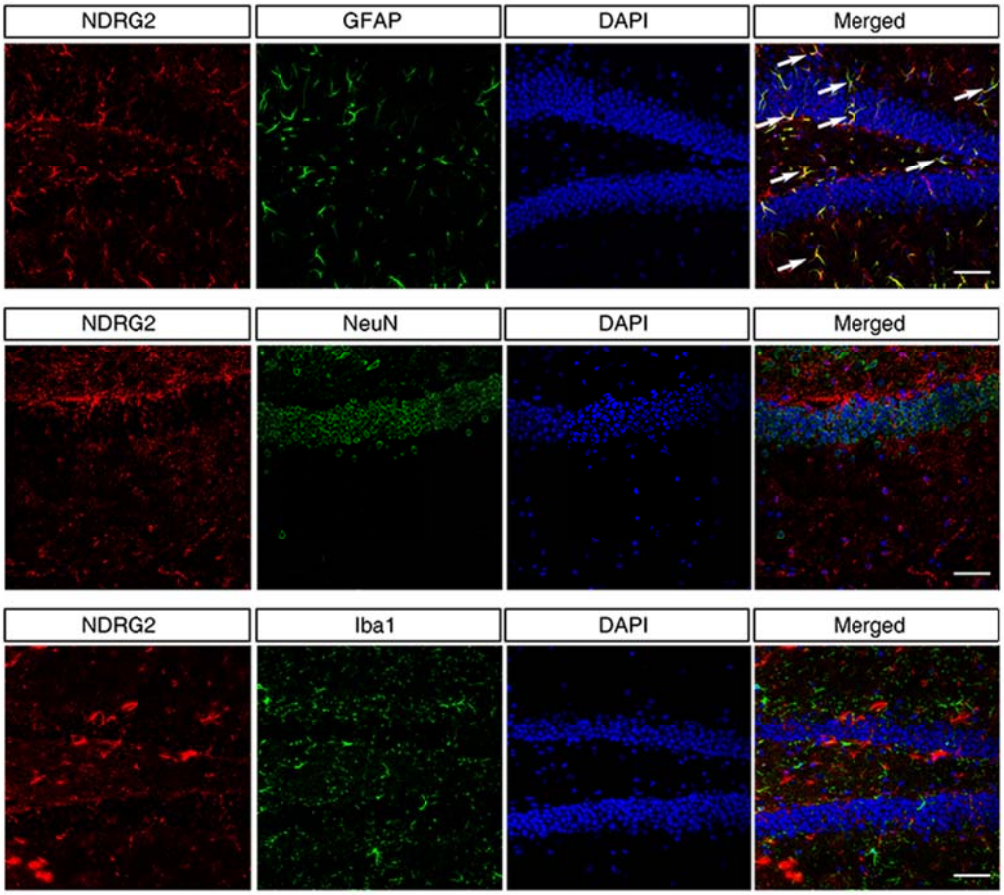

Supplemental Figure 14. NDRG2 is primarily expressed in astrocytes in the WT mouse brains. Representative fluorescence images of NDRG2 (red), GFAP (green), NeuN (green), Iba1 (green), and DAPI (blue) staining in the hippocampi of WT mice. Merged images are shown. White arrows show the colocalization of red and green fluorescence. Scale bar = 50 μm.

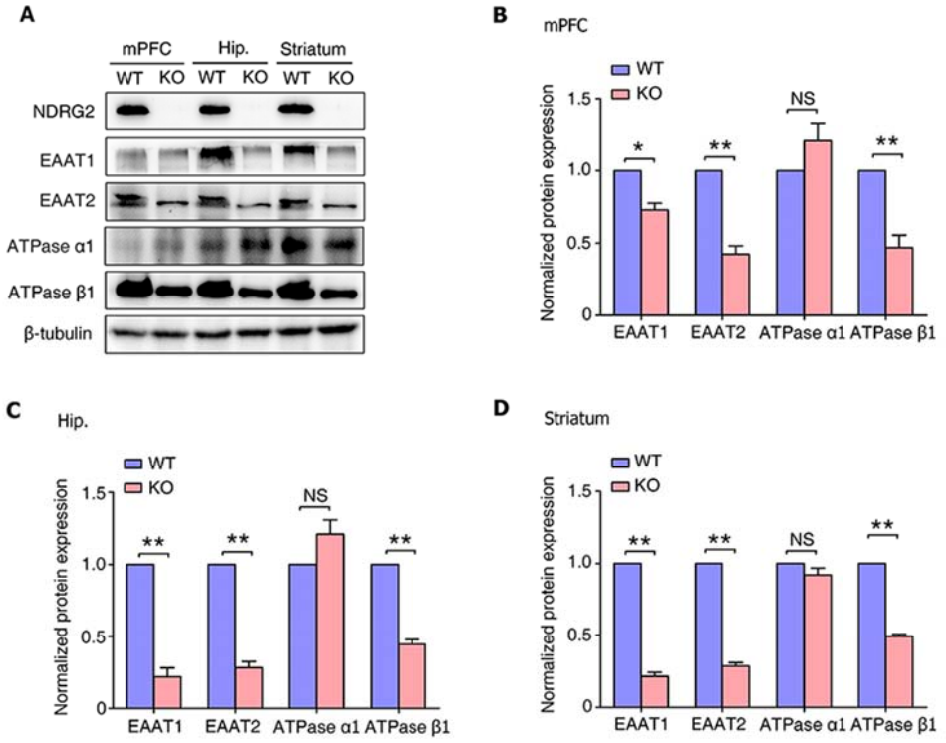

Supplemental Figure 15. Decreased levels of glutamate uptake-associated proteins in *Ndrg2*$^{-/-}$ mice. (**A**) Representative immunoblotting image of EAAT1, EAAT2, Na^+/K^+-ATPase α1 (ATPase α1), and Na^+/K^+-ATPase β1 (ATPase β1) in WT and *Ndrg2*$^{-/-}$ brains. The protein levels in the mPFC (**B**), hippocampus (**C**), or striatum (**D**) were analyzed by densitometry of immunoblots of whole-tissue lysates and were normalized to β-tubulin. Hip., hippocampus. $^{**}P < 0.01$; Student's *t*-test. Error bars indicate the mean ± SEM.

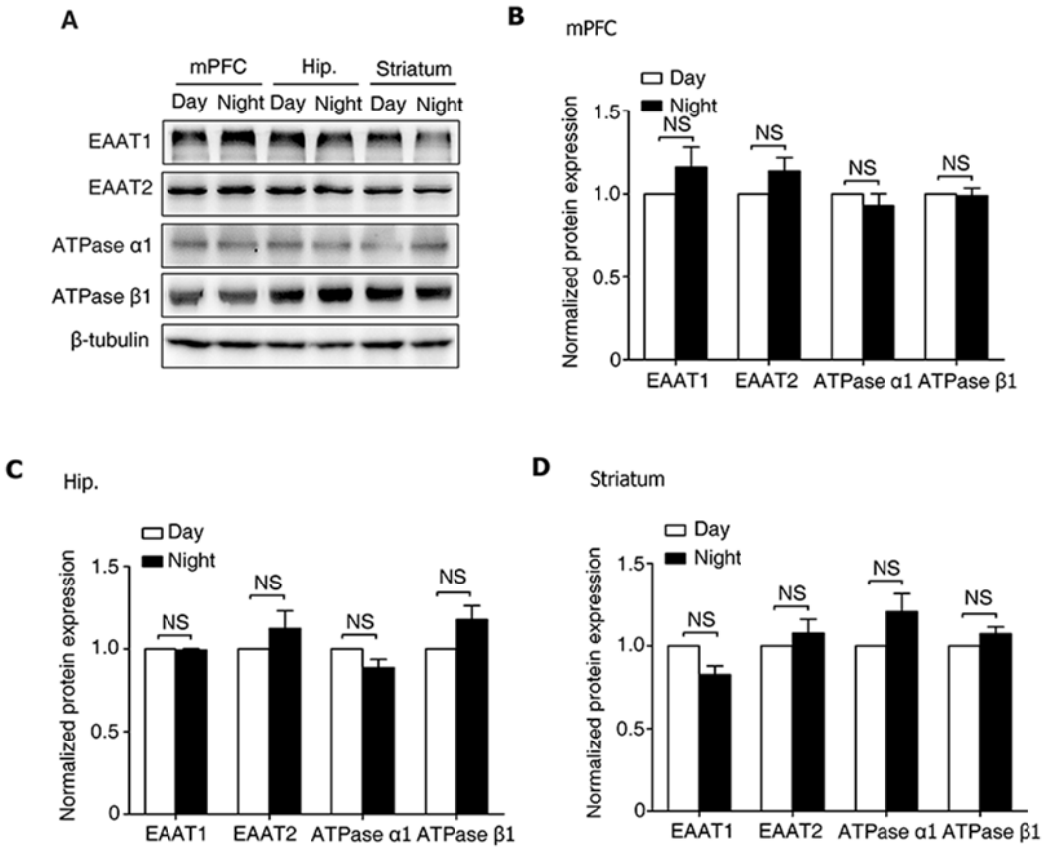

Supplemental Figure 16. No alteration in the levels of glutamate uptake-associated proteins between day and night in the *Ndrg2*$^{-/-}$ mice. (**A**) Representative immunoblotting image of EAAT1, EAAT2, Na^+/K^+-ATPase α1 (ATPase α1), and Na^+/K^+-ATPase β1 (ATPase β1) in the *Ndrg2*$^{-/-}$ brain during the day and night. The protein levels in the mPFC (**B**), hippocampus (**C**), or striatum (**D**) were analyzed by densitometry of immunoblots of whole-tissue lysates and were normalized to β-tubulin. Hip., hippocampus. Student's *t*-test. Error bars indicate the mean ± SEM.

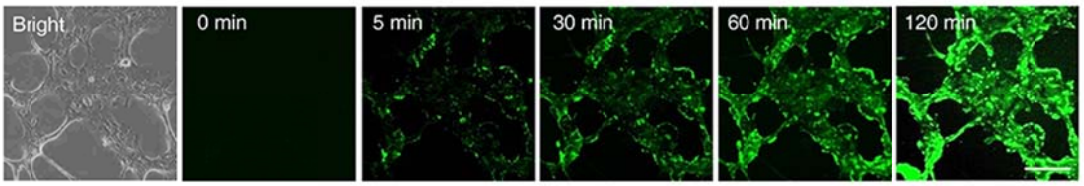

Supplemental Figure 17. Time course of TAT-NDRG2 (141-160)-FITC **treatment in vitro.** Fluorescence images from a representative experiment of TAT-NDRG2 (141-160)-FITC (20 μM) application to astrocyte cultures at 37 °C at various time intervals. Scale bar = 100 μm.

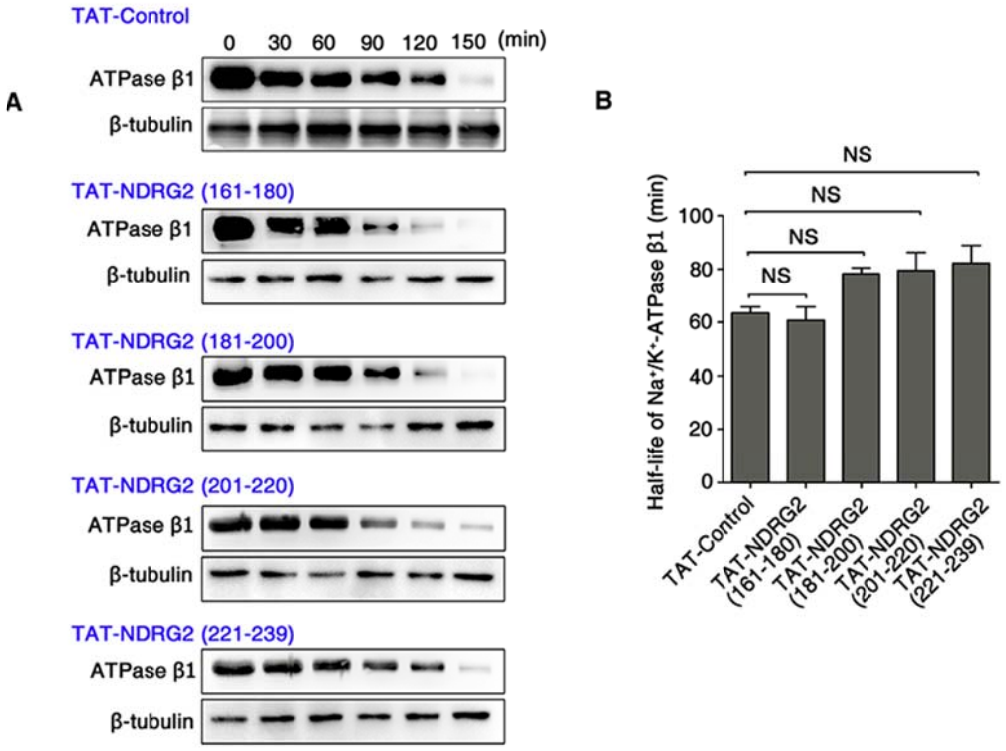

Supplemental Figure 18. Effects of NDRG2 peptides on the stability of the Na^+/K^+-ATPase β1 protein. (**A**) Na^+/K^+-ATPase β1 expression kinetics in the *Ndrg2*$^{-/-}$ astrocytes following the administration of the TAT-Control, TAT-NDRG2 (161-180), TAT-NDRG2 (181-200), TAT-NDRG2 (201-220), or TAT-NDRG2 (221-239) peptides with emetine. Representative immunoblots from three independent experiments are shown. (**B**) Quantification of the half-life of the Na^+/K^+-ATPase β1 protein at various time intervals in the kinetics analysis shown in (**A**). Error bars indicate the mean ± SEM; one-way ANOVA with the Tukey-Kramer *post hoc* test.

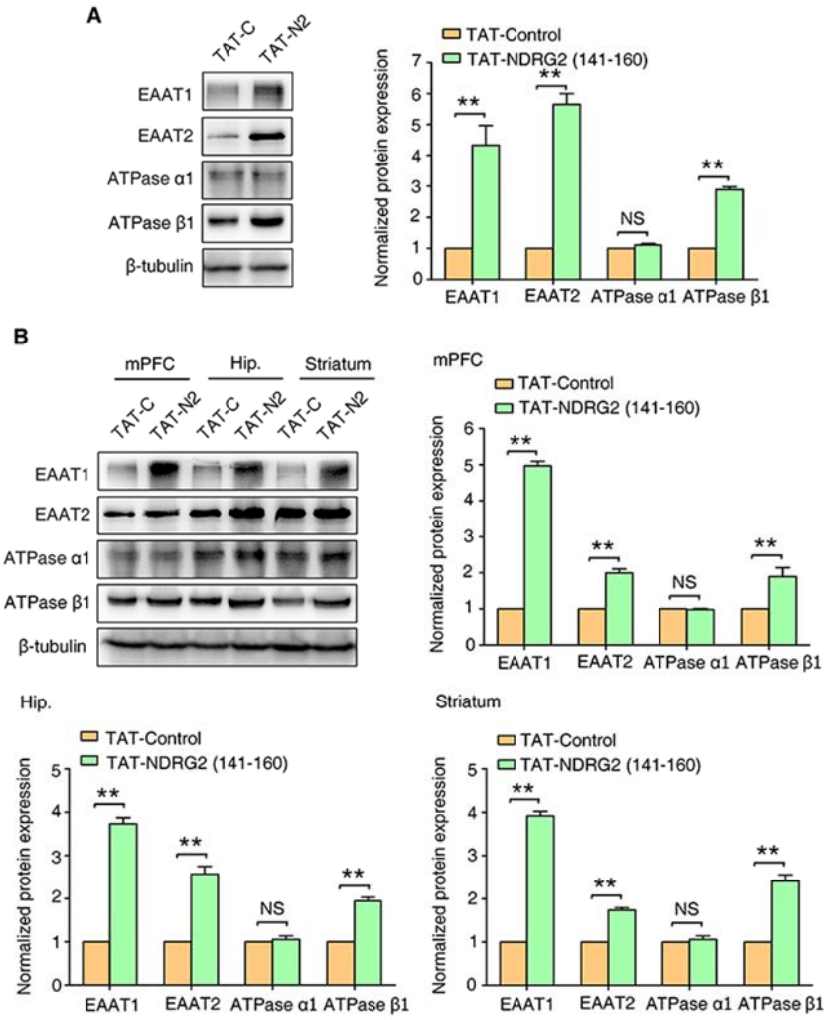

Supplemental Figure 19. The levels of glutamate uptake-associated proteins are rescued in the *Ndrg2*$^{-/-}$ astrocytes and *Ndrg2*$^{-/-}$ brains after TAT-NDRG2 (141-160) peptide treatment. The levels of the glutamate uptake-associated proteins NDRG2, EAAT1, EAAT2, Na^+/K^+-ATPase α1 (ATPase α1), and Na^+/K^+-ATPase β1 (ATPase β1) in the *Ndrg2*$^{-/-}$ astrocytes (**A**) and *Ndrg2*$^{-/-}$ brains (**B**) were analyzed by densitometry of immunoblots after TAT-Control or TAT-NDRG2 (141-160) peptide treatment. Representative immunoblots from three independent experiments are shown. TAT-C, TAT-Control; TAT-N2, TAT-NDRG2 (141-160). $^{**}P < 0.01$; Student's *t*-test. Error bars indicate the mean ± SEM.

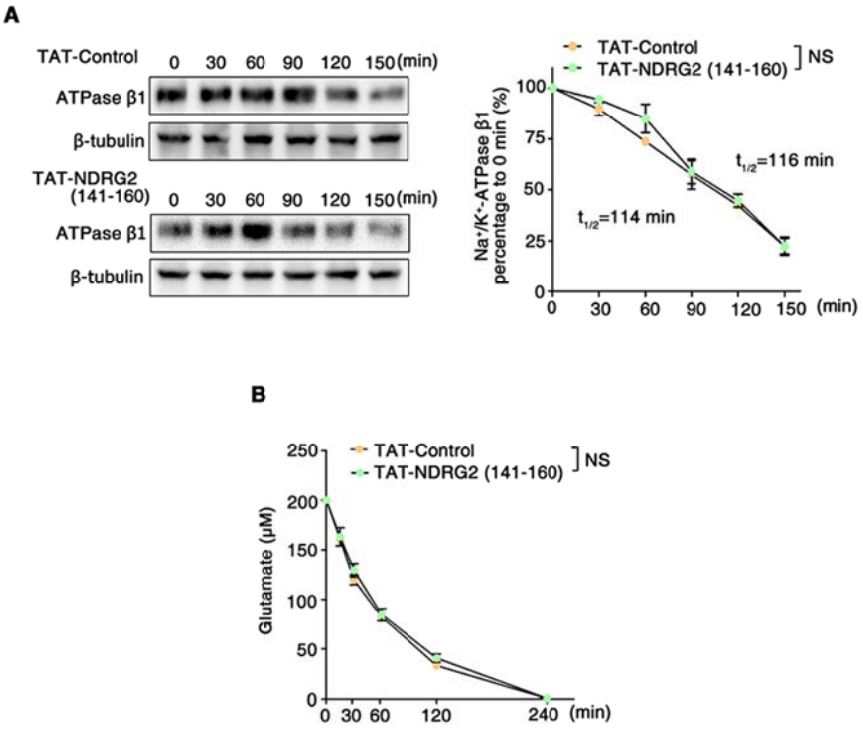

Supplemental Figure 20. No alterations in Na^+/K^+-ATPase β1 stability or glutamate uptake in the WT astrocytes after TAT-NDRG2 (141-160) treatment. (**A**) Na^+/K^+-ATPase β1 expression kinetics in the WT astrocytes following the administration of the TAT-Control or TAT-NDRG2 (141-160) peptide with emetine (a protein synthesis inhibitor). Representative immunoblots (left) from three independent experiments are shown. Relative Na^+/K^+-ATPase β1 levels normalized to β-tubulin levels were quantified by densitometry at various time intervals (right). Repeated-measures ANOVA. (**B**) Glutamate levels in the media of cultured WT astrocytes were measured at various time intervals following the administration of the TAT-Control or TAT-NDRG2 (141-160) peptide. Data were obtained from three independent measurements, and each experiment was performed in quadruplicate. Repeated-measures ANOVA.

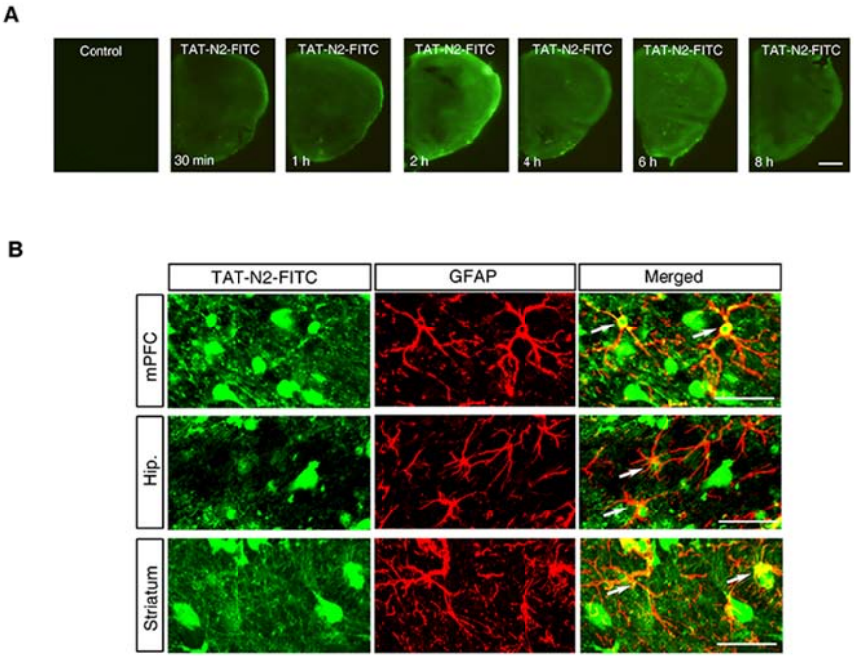

Supplemental Figure 21. Time course of TAT-NDRG2 (141-160)-FITC treatment and TAT-NDRG2 (141-160)-FITC distribution in vivo. (**A**) Representative fluorescence images of half-brain slices after TAT-NDRG2 (141-160)-FITC injection into the *Ndrg2*$^{-/-}$ mice by subclavian vein at various time intervals. Scale bar = 1mm. (**B**) Representative fluorescence images of GFAP (red) and FITC (green) staining in the *Ndrg2*$^{-/-}$ brains 2 hours after TAT-NDRG2 (141-160) -FITC injection. Merged images are shown. White arrows showed the colocalization of red and green fluorescence. Scale bar = 50 μm. TAT-N2-FITC, TAT-NDRG2 (141-160)-FITC.

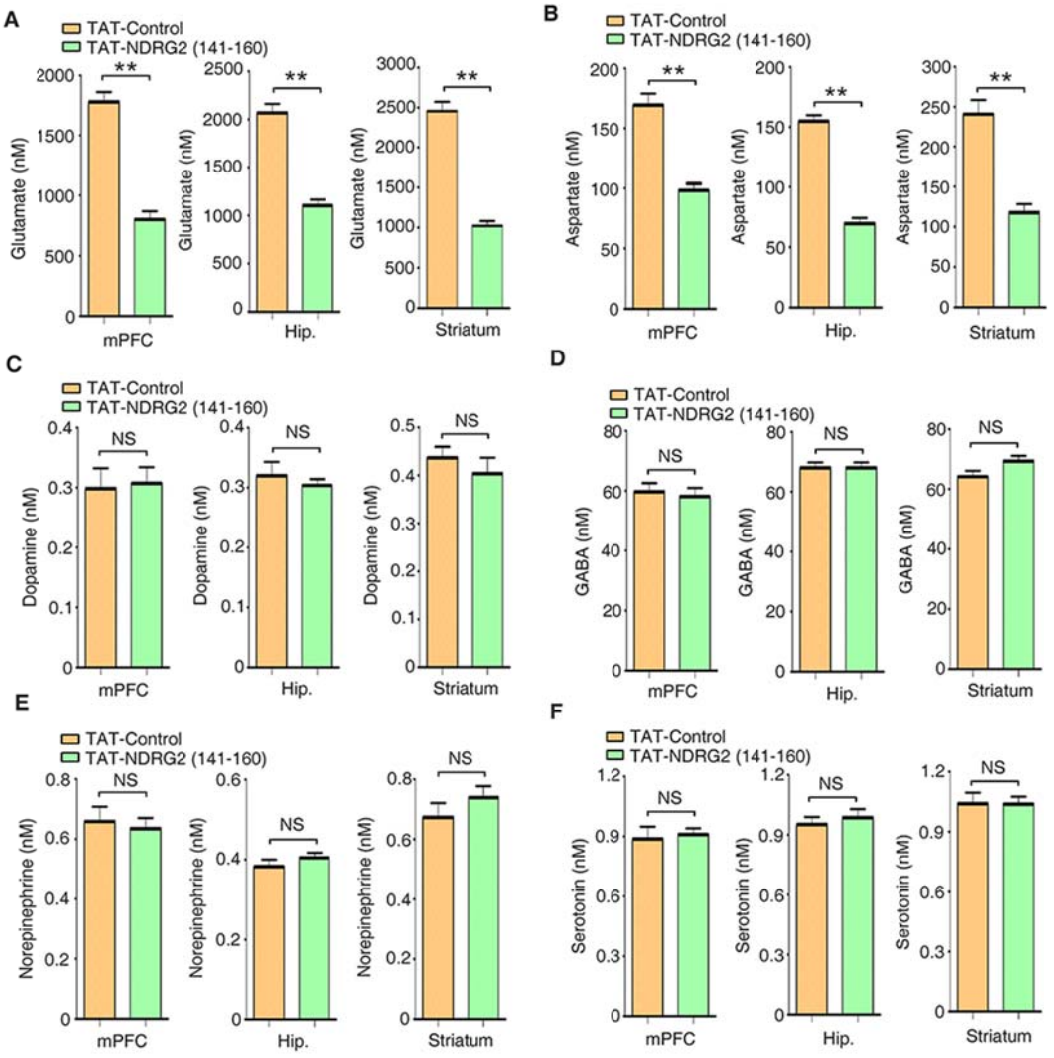

Supplemental Figure 22. The NDRG2 peptide rescues the increased interstitial glutamate and aspartate levels in the *Ndrg2*$^{-/-}$ mice. Measurements of interstitial glutamate (**A**), aspartate (**B**), dopamine (**C**), GABA (**D**), norepinephrine (**E**), and serotonin concentrations (**F**) in the mPFC, hippocampus, or striatum in the *Ndrg2*$^{-/-}$ mice that were injected with the TAT-Control or TAT-NDRG2 (141-160) peptide. n = 6 per group; $^{**}P < 0.01$; error bars, mean ± SEM; Student's *t*-test.

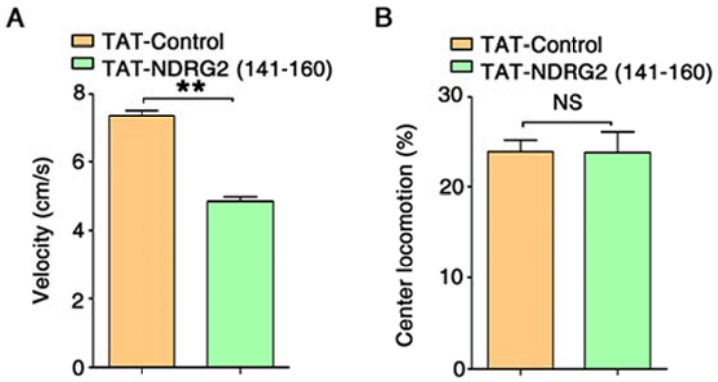

Supplemental Figure 23. The NDRG2 peptide corrects the elevated velocity in the *Ndrg2*$^{-/-}$ mice in the open field test. Effects of the TAT-Control and TAT-NDRG2 (141-160) peptides on the velocity (**A**) and center locomotion (**B**) in the *Ndrg2*$^{-/-}$ mice. n = 9 per group; $^{*}P < 0.05$; error bars, mean ± SEM; Student's *t*-test.

Supplemental Tables

Supplemental Table 1. 5-CSRTT training schedule.

Level	Delay (s)	Cue (s)	Response (s)	Criteria
1	2	30	10	≥ 30 Correct responses
2	2	20	10	≥ 30 Correct responses
3	5	10	5	≥ 40 Correct responses
4	5	5	5	≥ 50 Correct responses
5	3/4/5	2	5	≥ 50 Correct responses and ≤ 20% omitted responses
6	3/4/5	1	5	≥ 50 Correct responses and ≤ 20% omitted responses

Supplemental Table 2. Sources and dilutions of the antibodies used in the study.

Antigen	Dilution	Source	Application	Catalog number
NDRG2	1:1,000	CST	IB	#5667
	1:100	Abcam	IF	ab174850
EAAT1	1:1,000	Abcam	IB	ab181036
EAAT2	1:1,000	Abcam	IB	ab178401
Na^+/K^+-ATPase α1	1:1,000	CST	IB	#23565
Na^+/K^+-ATPase β1	1:1,000	Abcam	IB	ab193669
Flag-tag	1:50	CST	IP	#2368
Myc-tag	1:50	CST	IP	#2276
NeuN	1:400	Millipore	IF	MAB377
GFAP	1:150	CST	IF	#3670
Iba1	1:50	Abcam	IF	ab5076
NR1	1:500	Abcam	IB	ab109182
NR2A	1:1,000	CST	IB	#4205
NR2B	1:1,000	CST	IB	#4207
GluR1	1:1,000	CST	IB	#8652 Kit
GluR2	1:1,000	CST	IB	#8652 Kit
GluR3	1:1,000	CST	IB	#8652 Kit
β-tubulin	1:2,000	CST	IB	#2128

CST, Cell Signaling Technology; IB, immunoblotting; IF, immunofluorescence, IP, immunoprecipitation.

Supplemental References

1. Won, H., Mah, W., Kim, E., Kim, J.W., Hahm, E.K., Kim, M.H., Cho, S., Kim, J., Jang, H., Cho, S.C., et al. 2011. GIT1 is associated with ADHD in humans and ADHD-like behaviors in mice. *Nat Med* 17:566-572.
2. Wells, M.F., Wimmer, R.D., Schmitt, L.I., Feng, G., and Halassa, M.M. 2016. Thalamic reticular impairment underlies attention deficit in Ptchd1(Y/-) mice. *Nature* 532:58-63.
3. Kondziella, W. 1964. [a New Method for the Measurement of Muscle Relaxation in White Mice]. *Arch Int Pharmacodyn Ther* 152:277-284.

Full unedited gel for Figure 3B

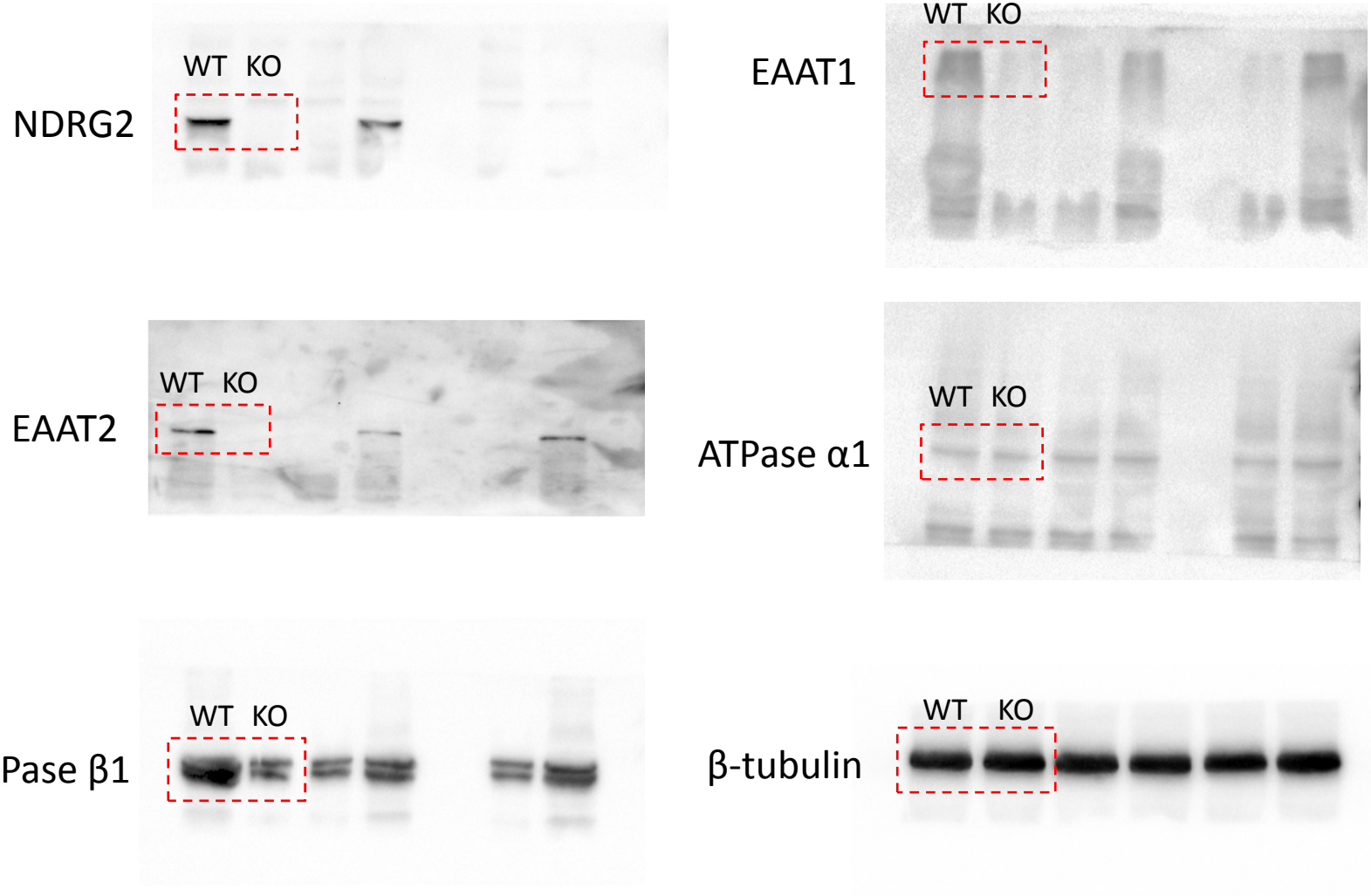

Full unedited gel for Figure 3C

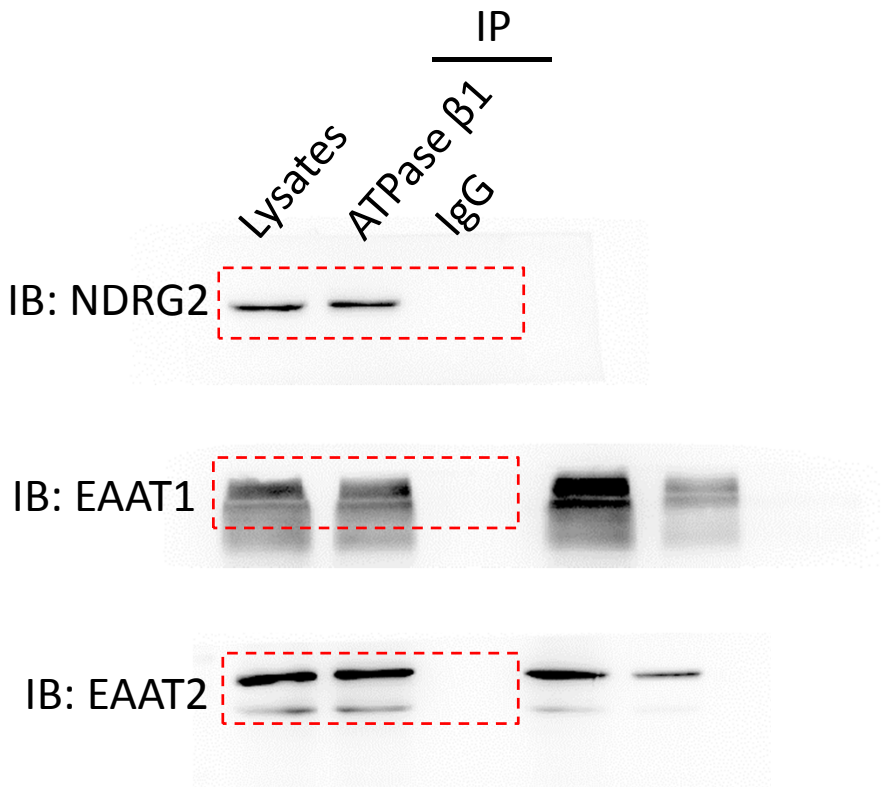

Full unedited gel for Figure 3D

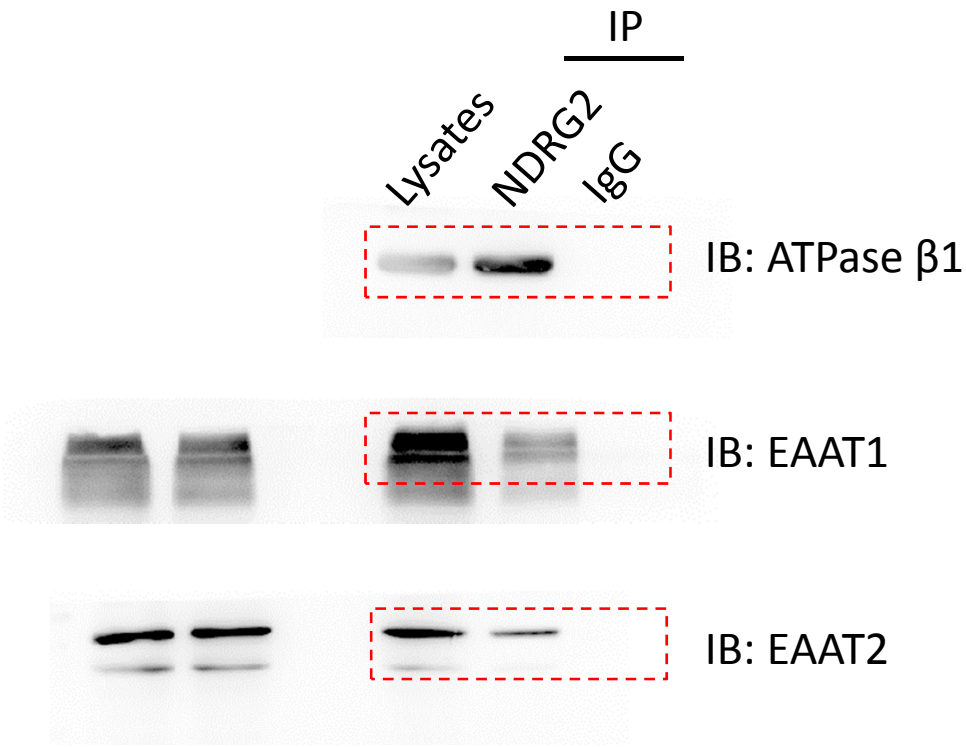

Full unedited gel for Figure 3E

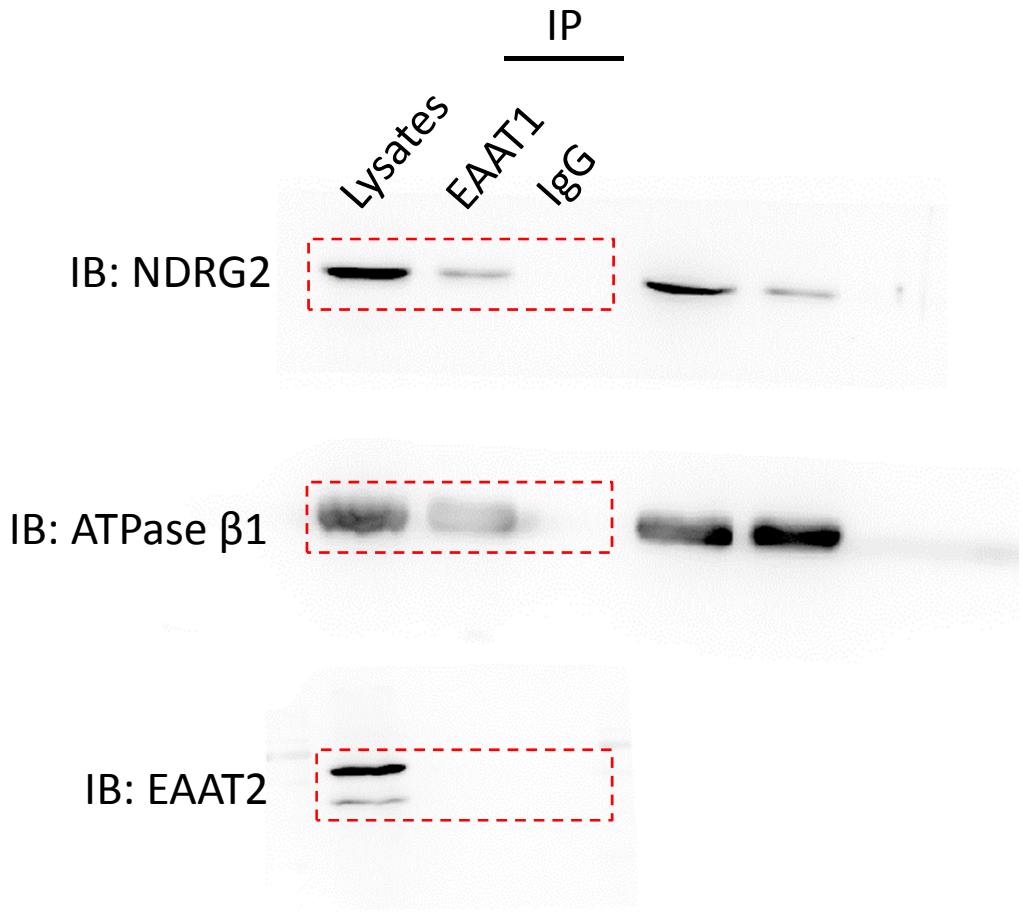

Full unedited gel for Figure 3F

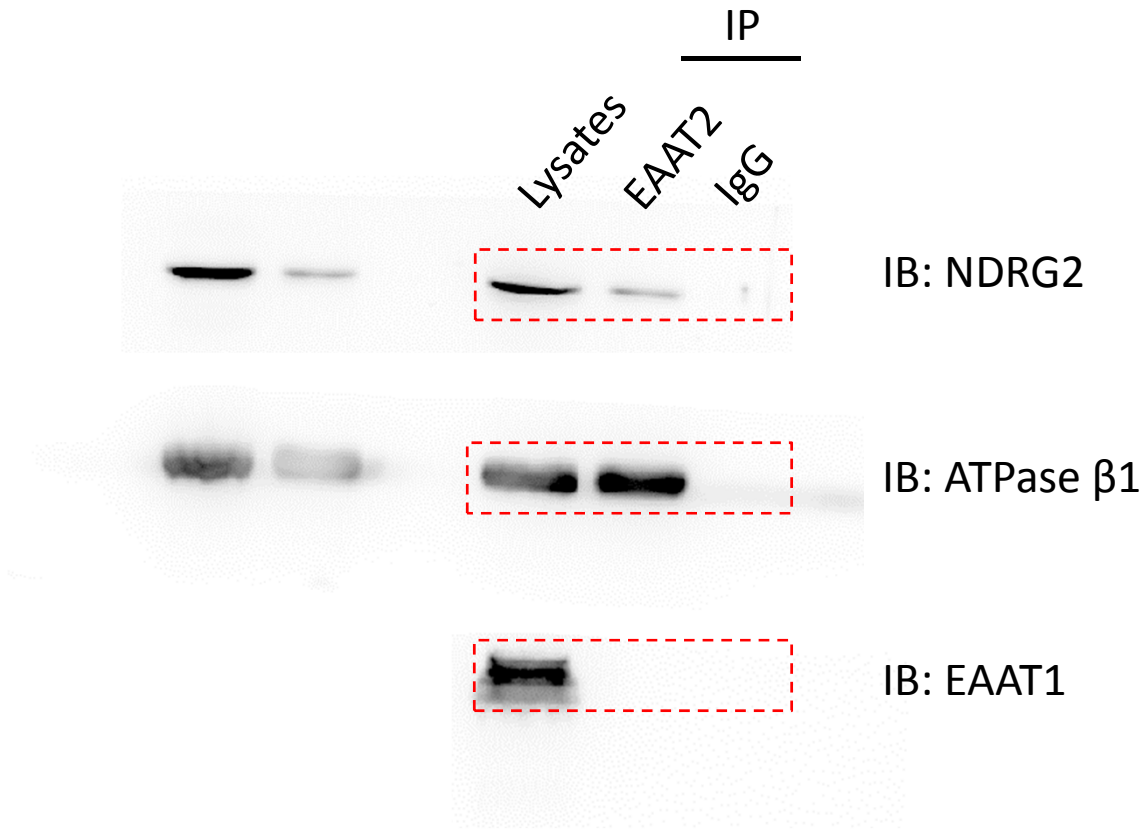

Full unedited gel for Figure 3G

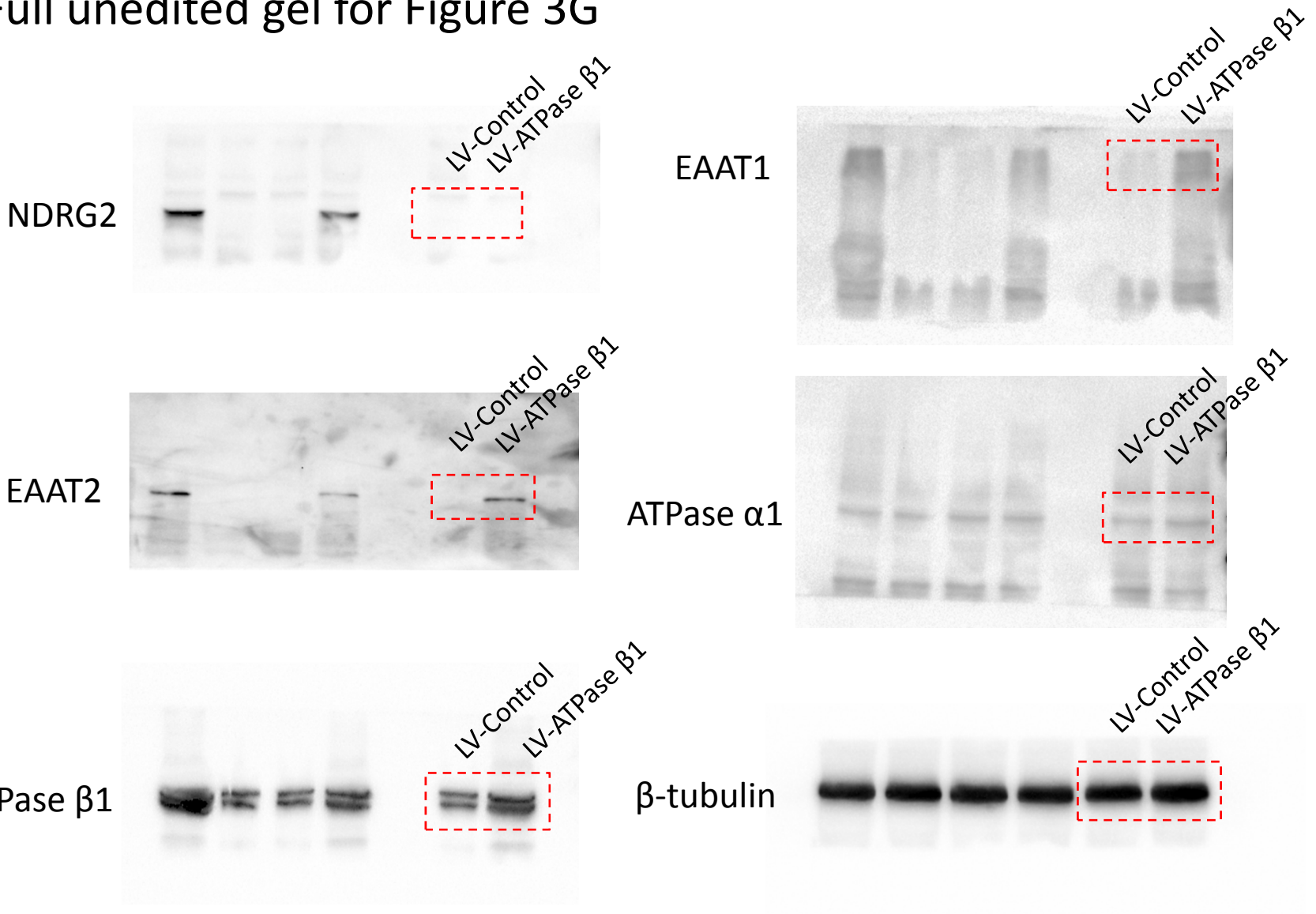

Full unedited gel for Figure 4A

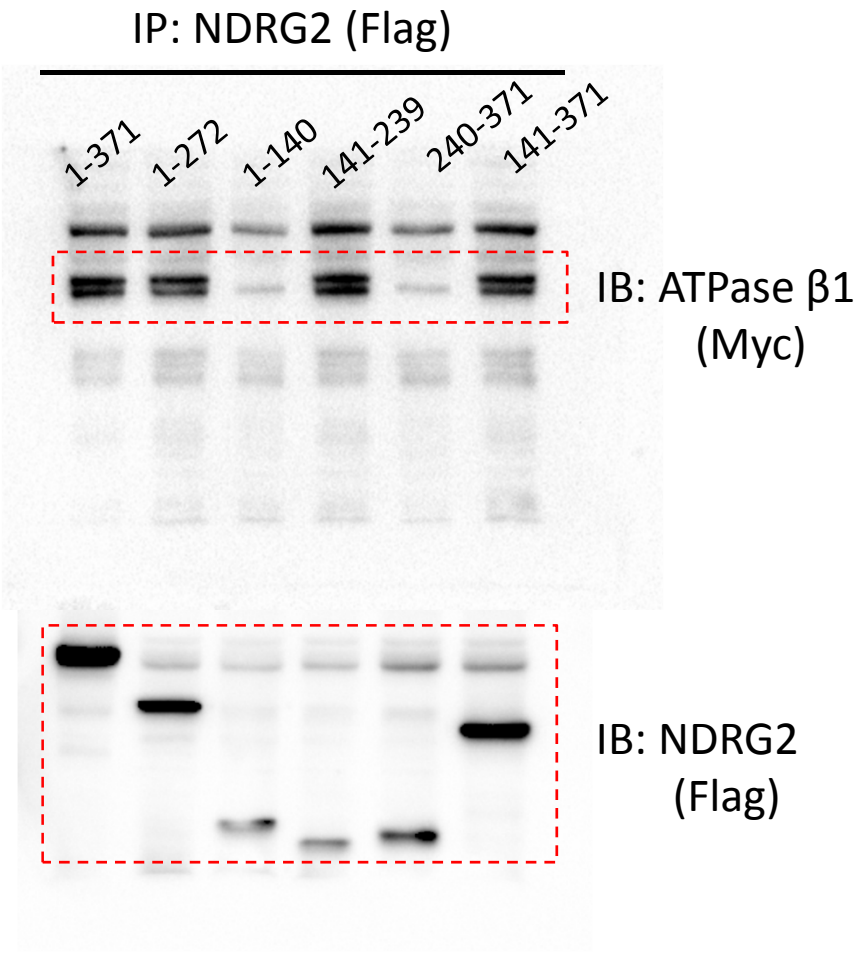

Full unedited gel for Figure 4B

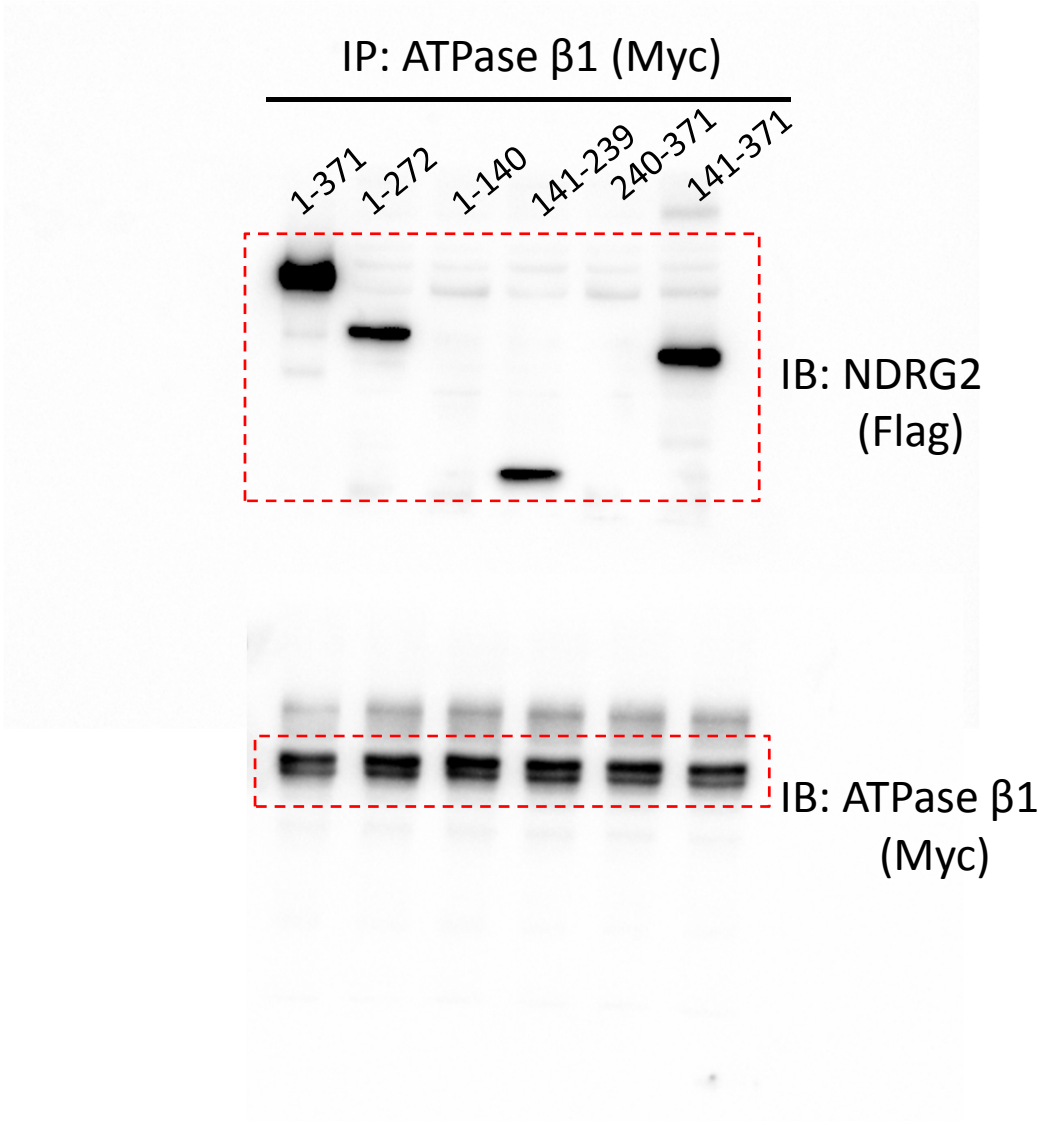

Full unedited gel for Figure 4E

TAT-Control

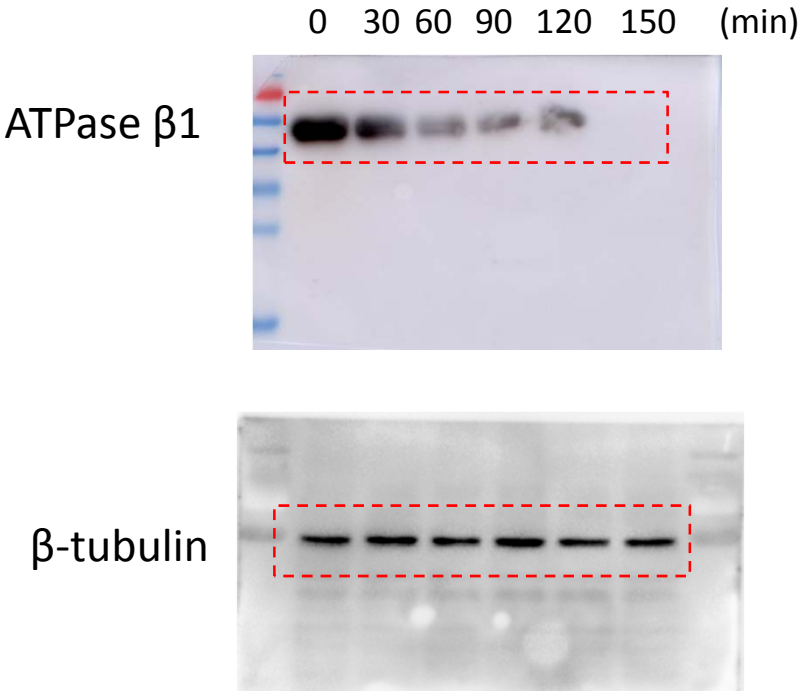

TAT-NDRG2(141-160)

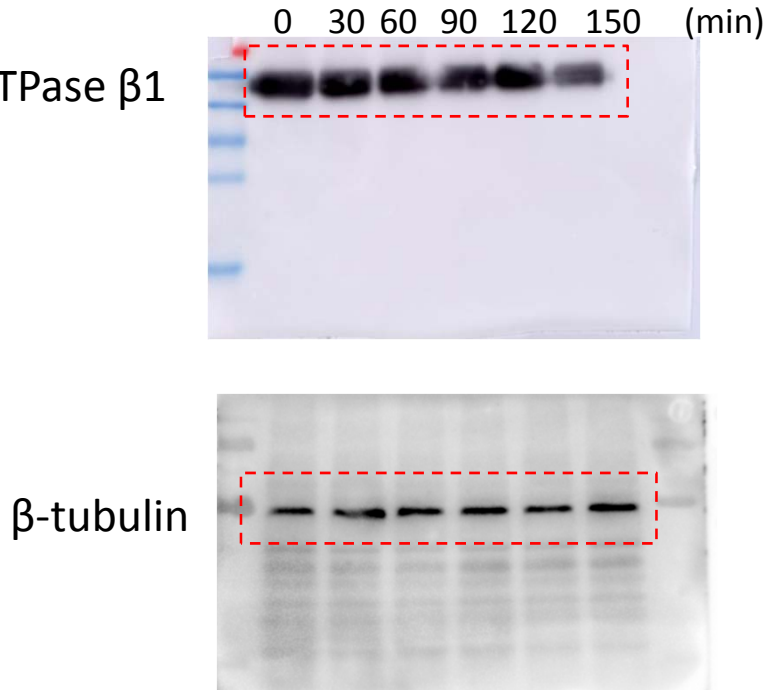

Full unedited gel for Supplemental Figure 12A

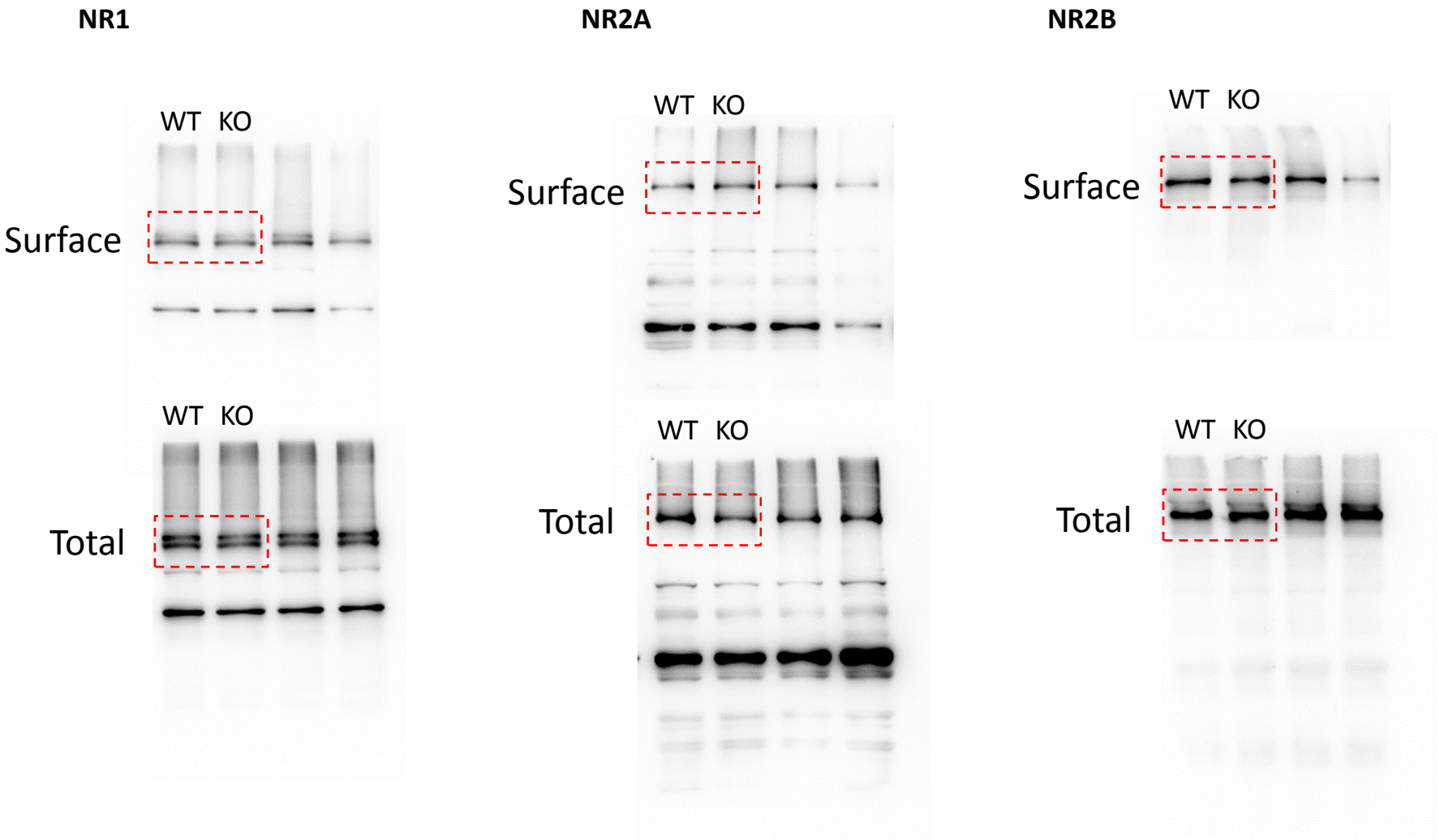

Full unedited gel for Supplemental Figure 12B

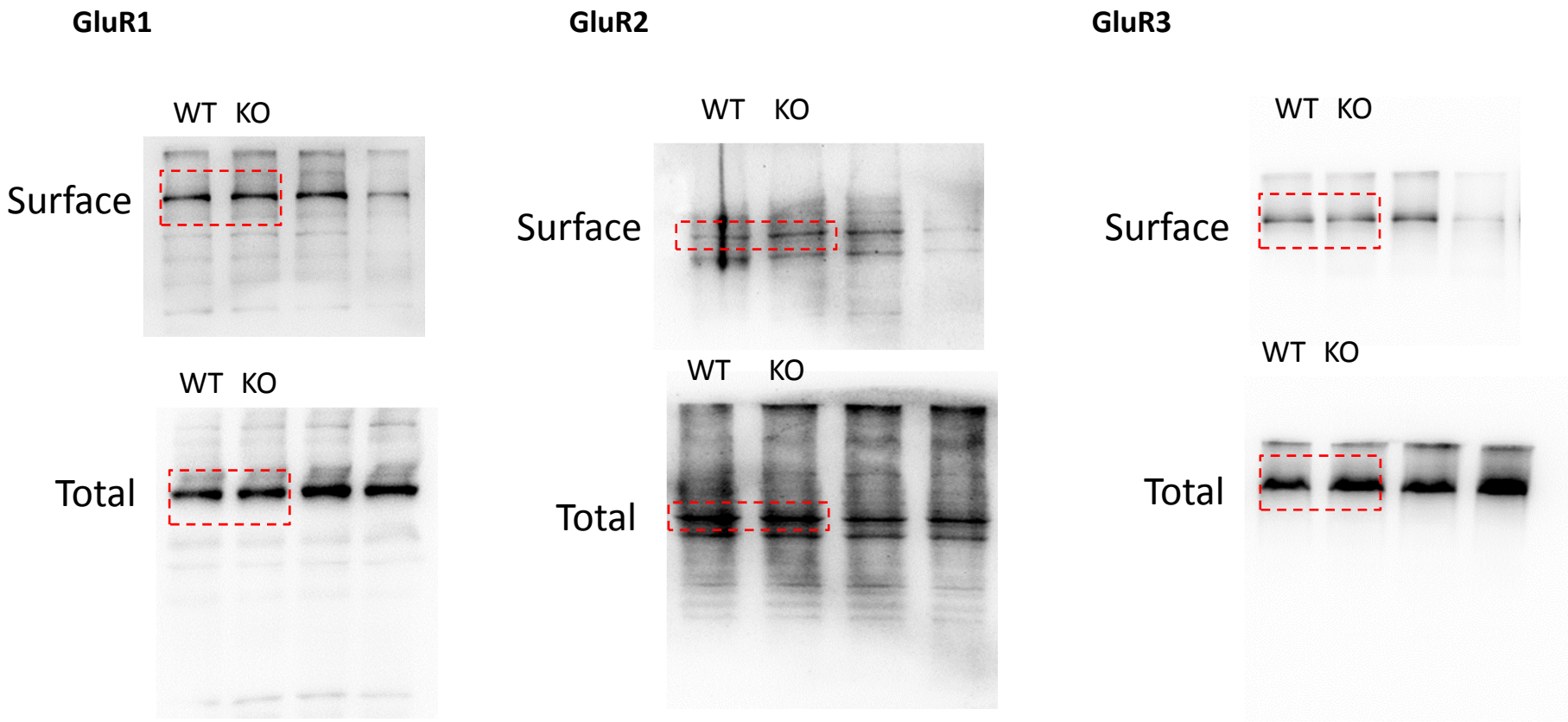

Full unedited gel for Supplemental Figure 13D

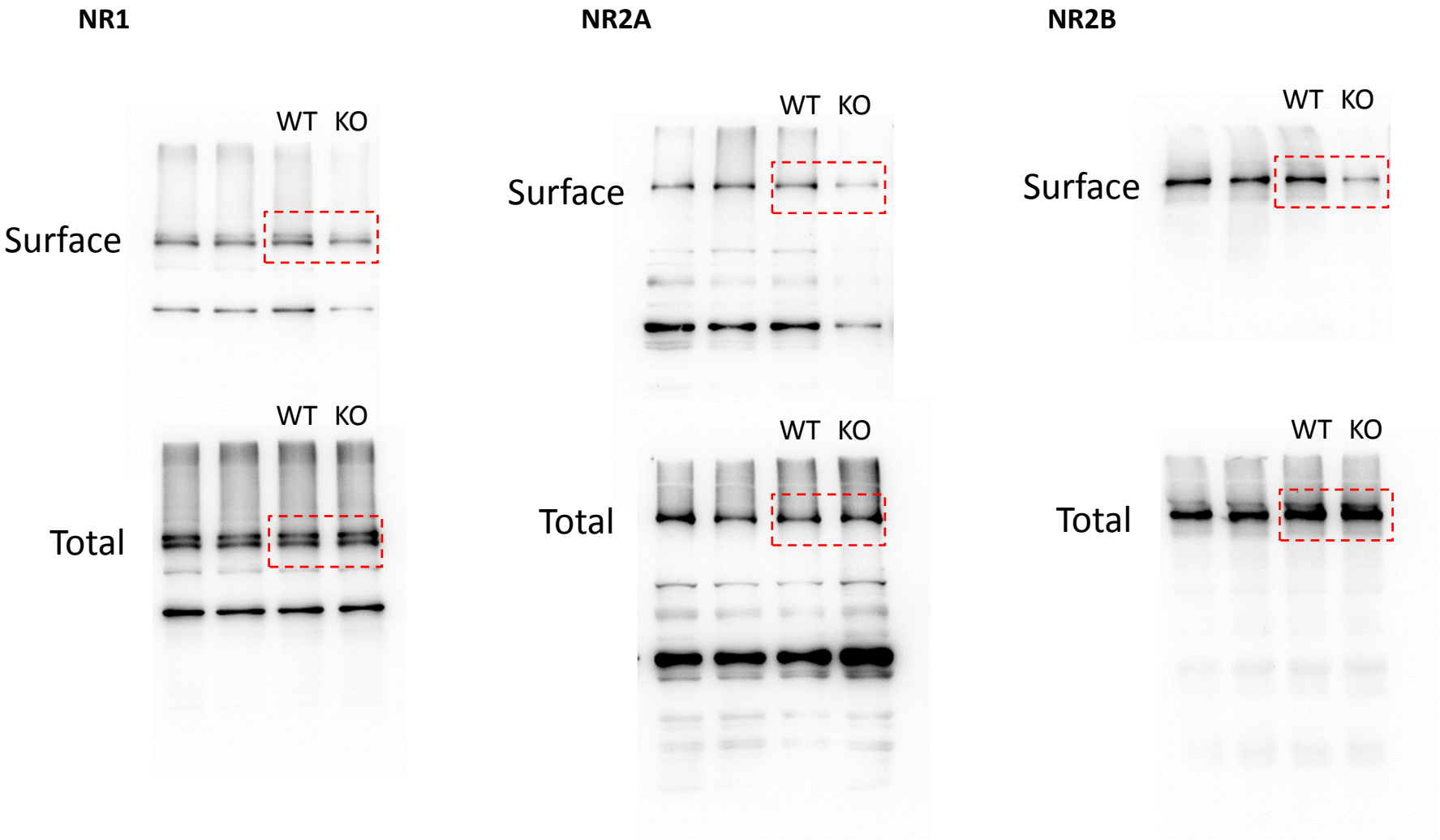

Full unedited gel for Supplemental Figure 13E

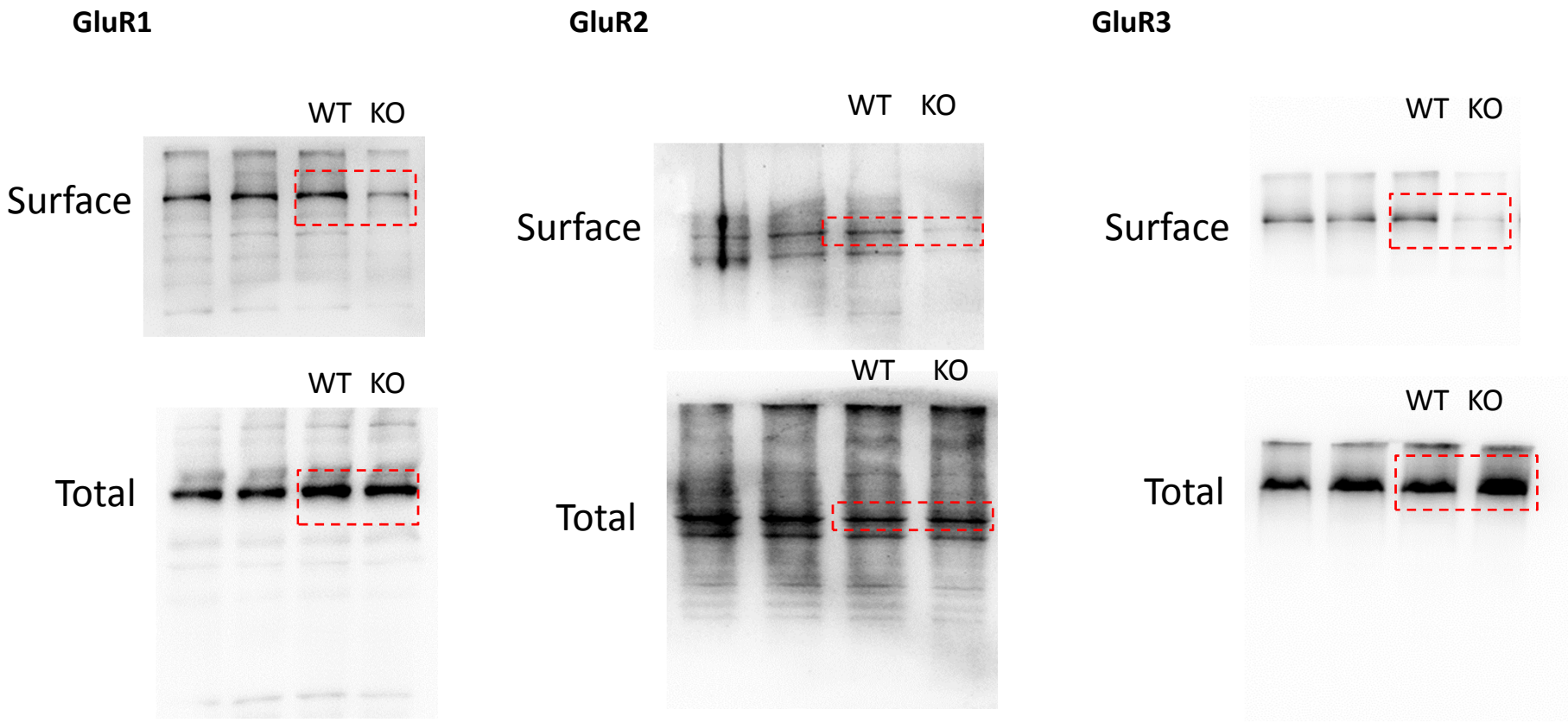

Full unedited gel for Supplemental Figure 15A

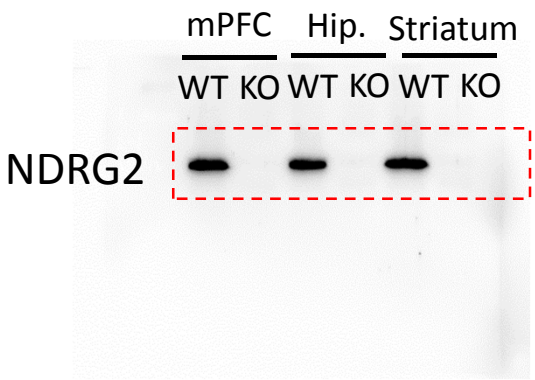

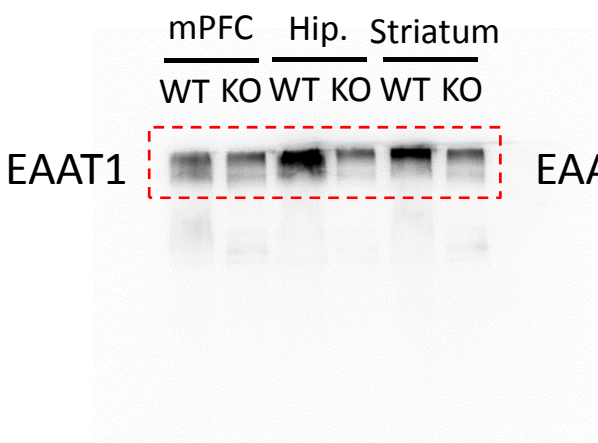

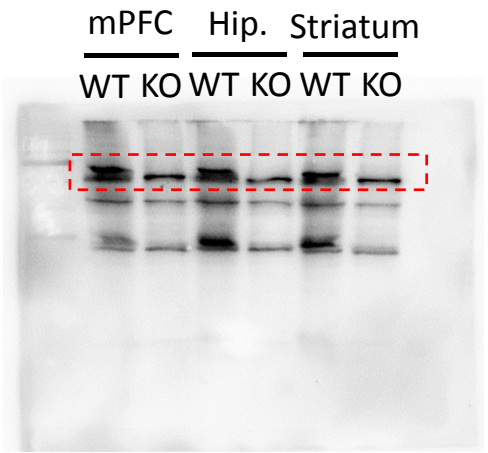

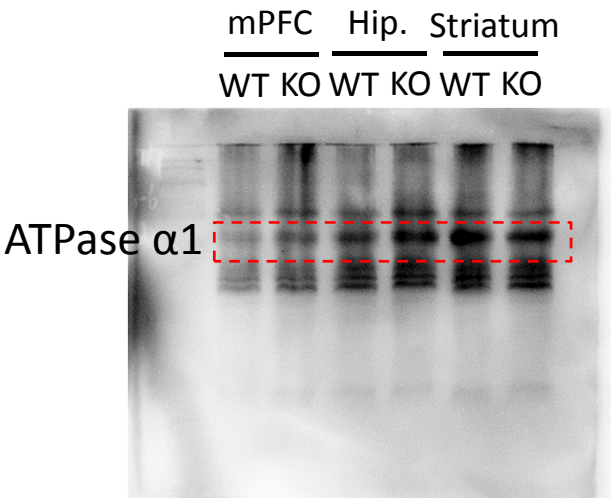

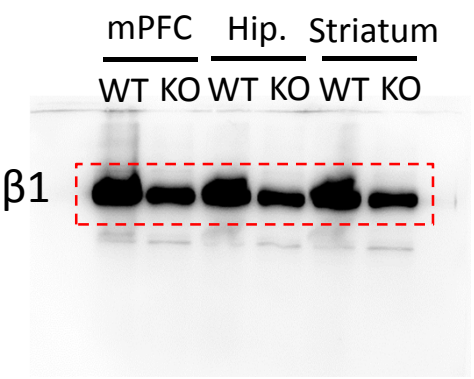

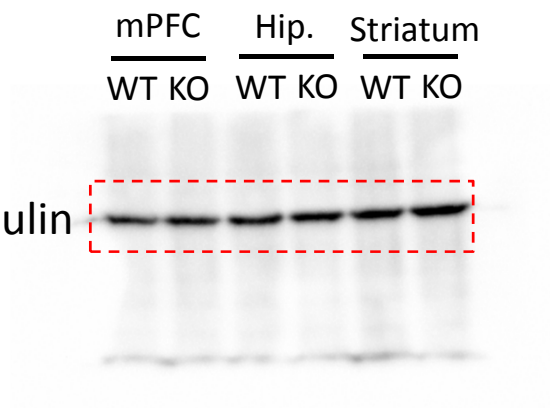

Full unedited gel for Supplemental Figure 16A

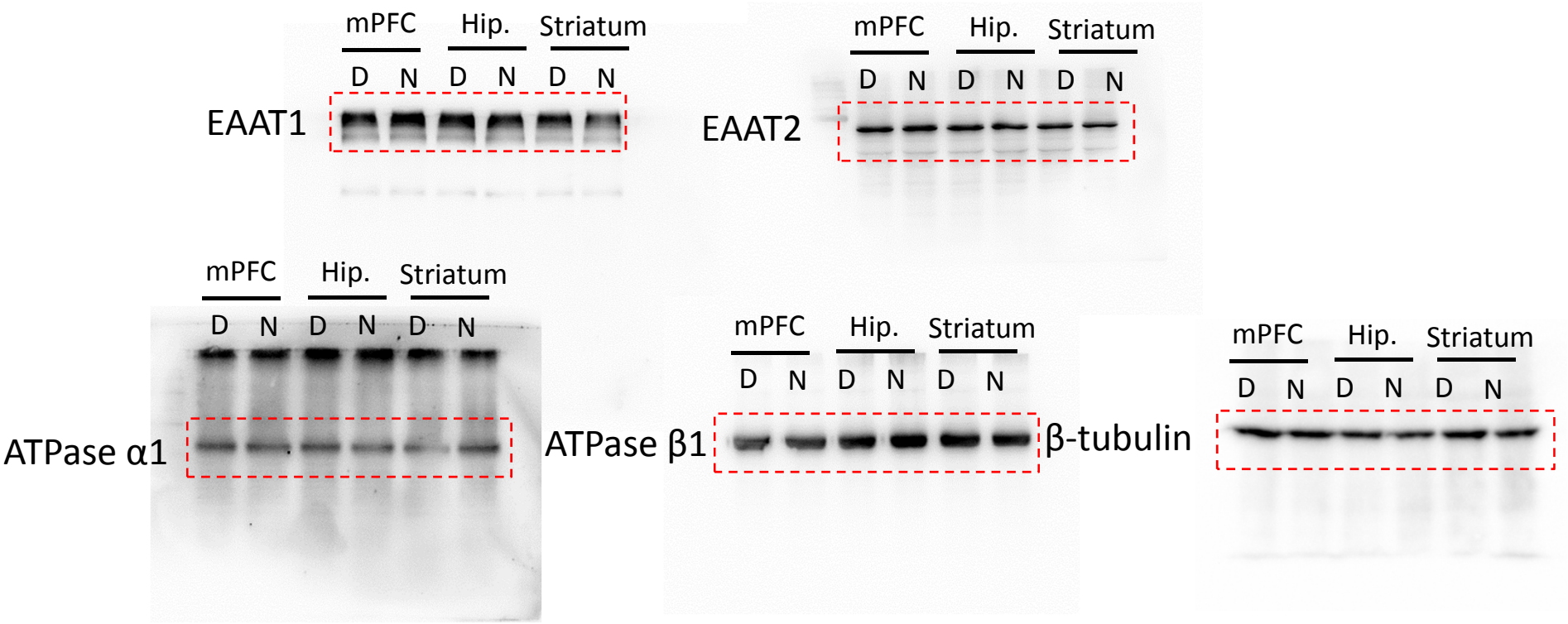

Full unedited gel for Supplemental Figure 18

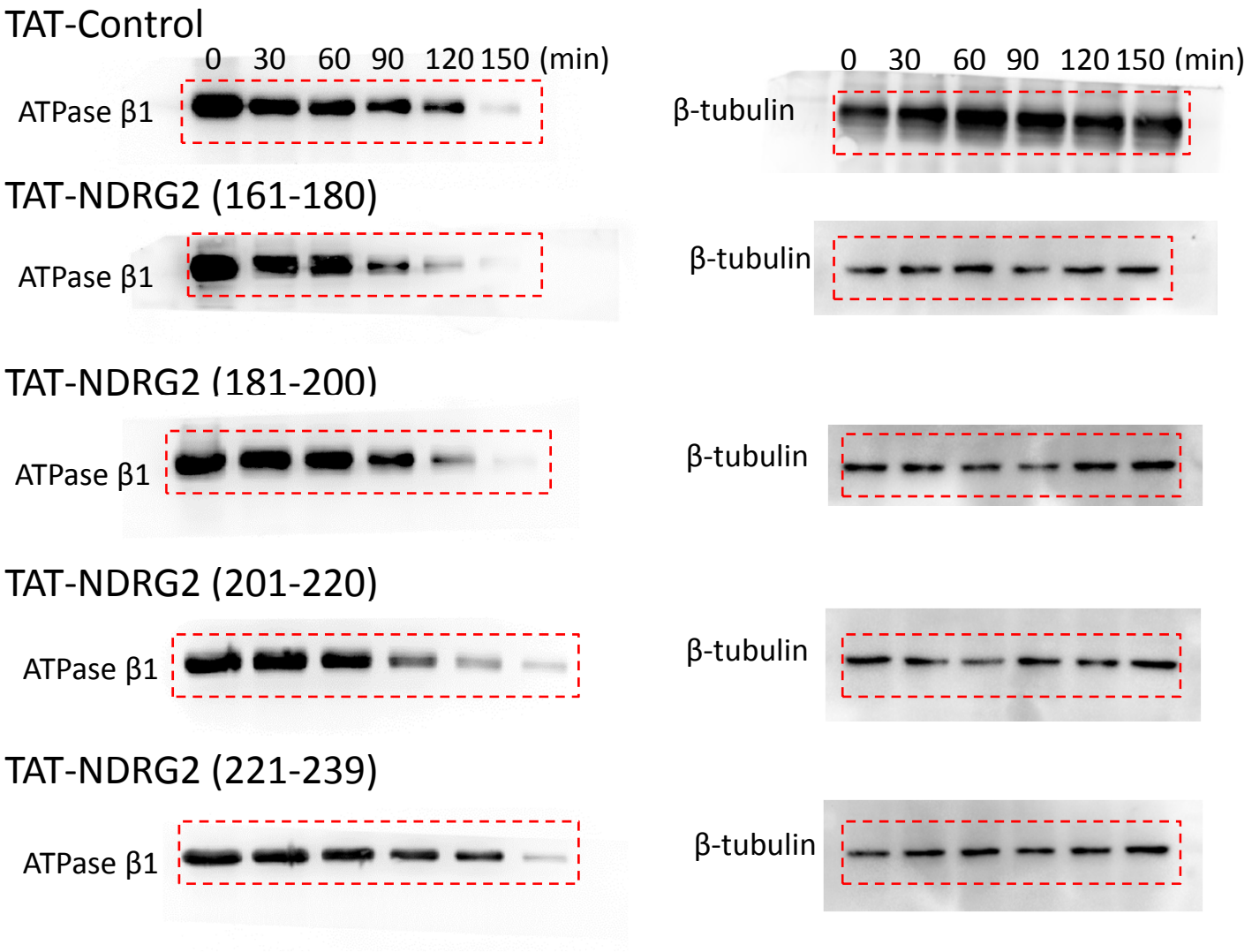

Full unedited gel for Supplemental Figure 19A

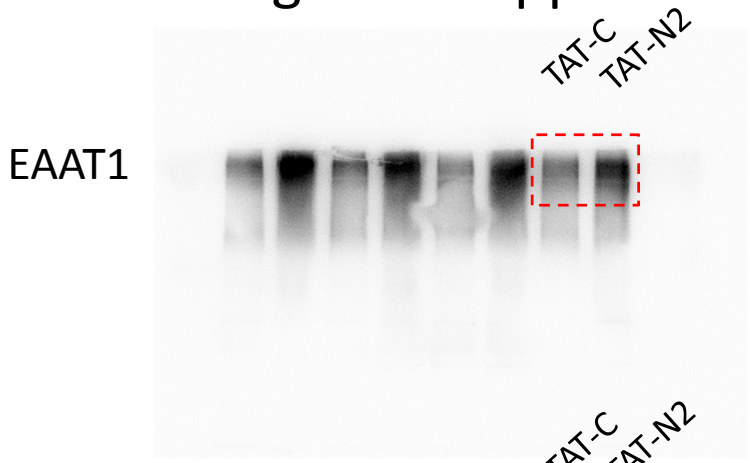

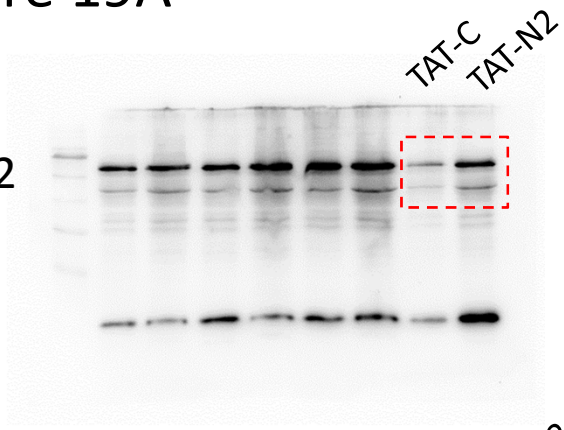

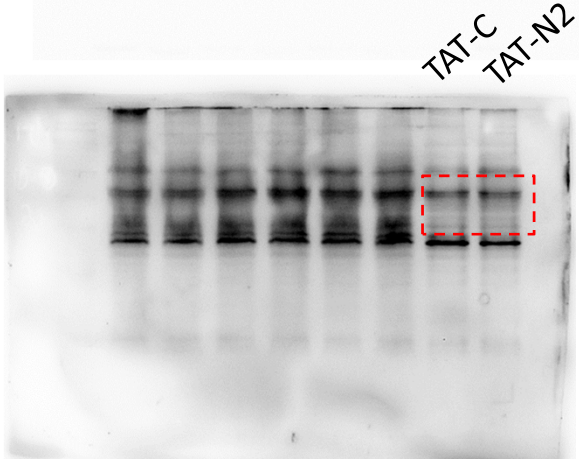

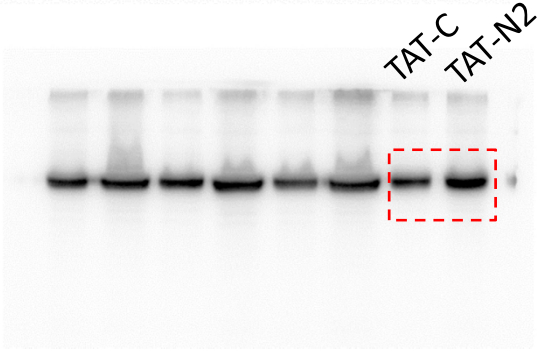

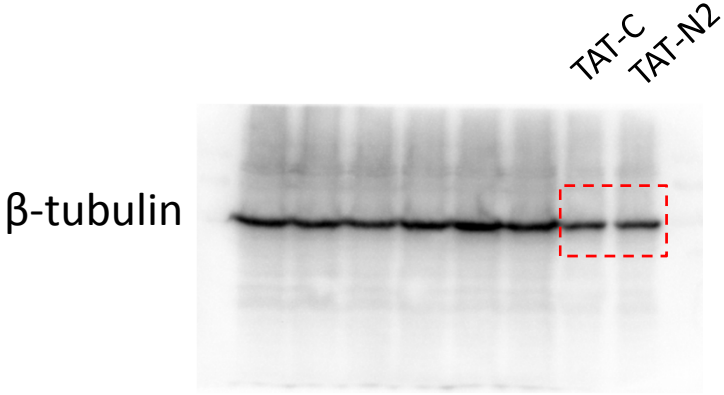

Full unedited gel for Supplemental Figure 19B

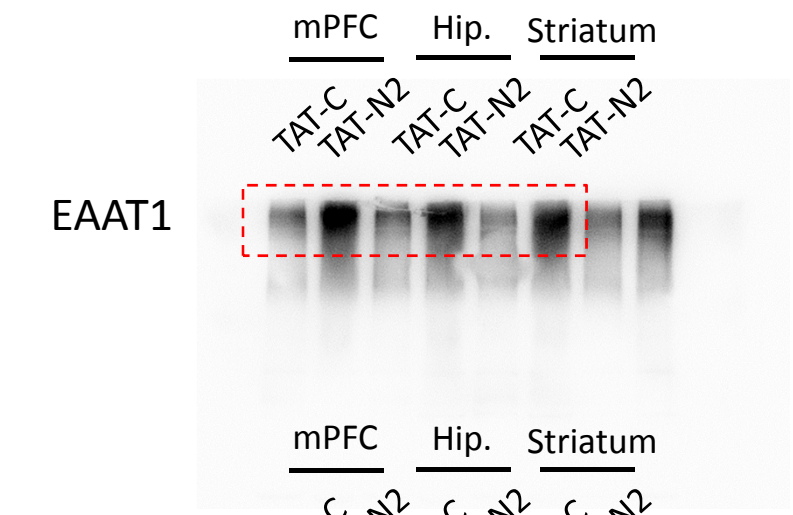

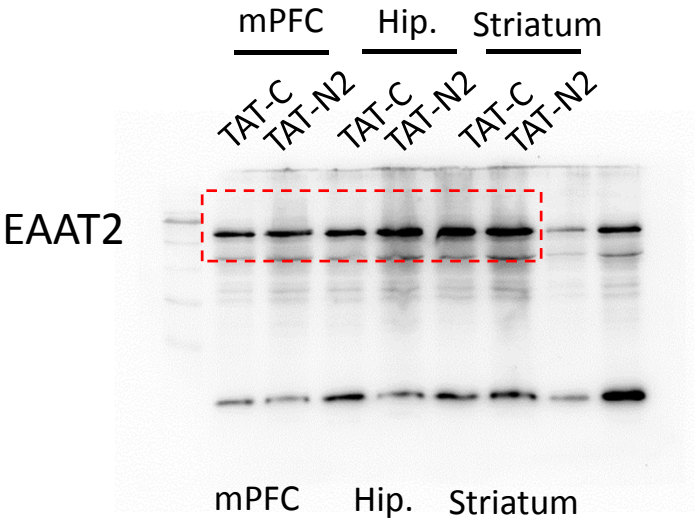

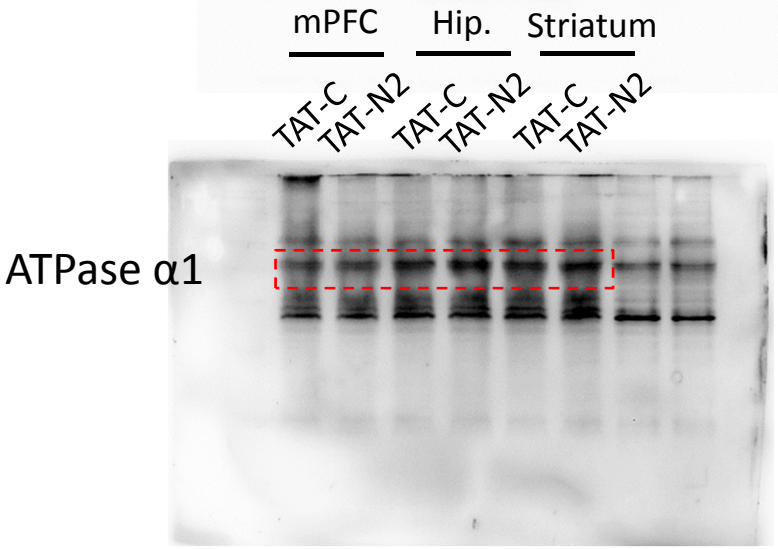

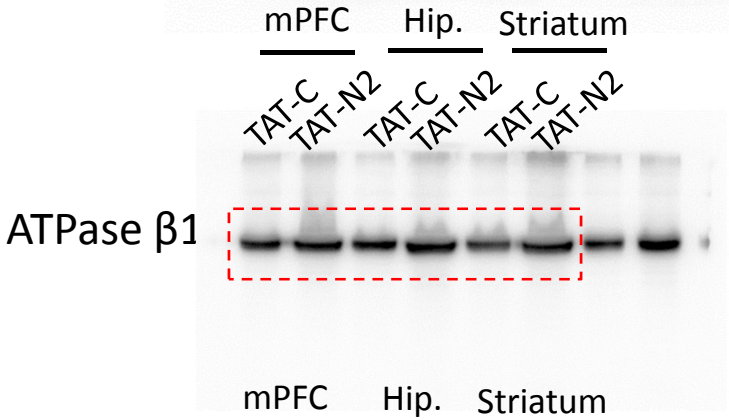

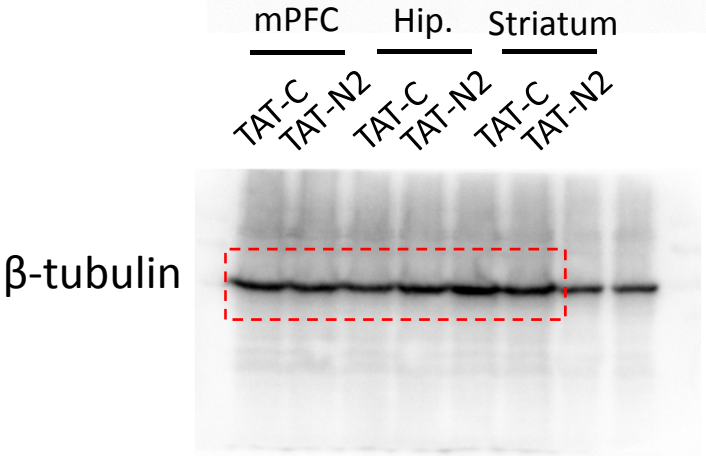

Full unedited gel for Supplemental Figure 20A

TAT-Control

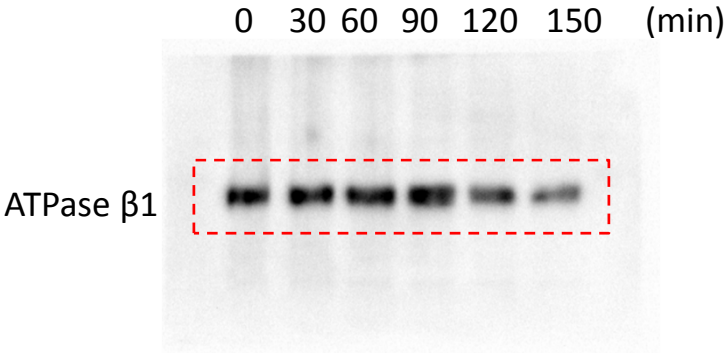

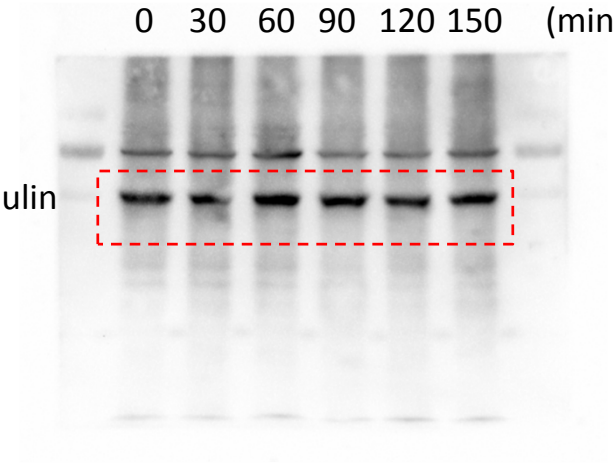

TAT-NDRG2(141-160)